ERDC TN-DOER-N16
August 2002

Sediment Dispersion Near Dredge Pipeline Discharge in Laguna Madre, Texas

PURPOSE: Results of field measurements taken near a pipeline discharge of fine-grained dredged material into shallow water, a revised numerical model formulation, and comparisons between field and model results are presented herein. A numerical model for the simulation of underflow spreading resulting from a pipeline disposal was previously presented in TN-DOER-N11 (Teeter 2001). That model is updated here, guided by the analysis of field measurements. An analysis of entrainment of underflow material into the water column under the action of wind-waves is also presented.

BACKGROUND: Initial dispersion of dredged material after pipeline discharge is important to deposit area and susceptibility to erosion or resuspension. Dispersion consists of a fluid-mud gravity underflow and, possibly, an overlying water-column plume. Fluid-mud thickness, concentration structure, and overlying water-column suspension concentration were measured in shallow, wind-exposed, micro-tidal Laguna Madre, TX, within about 500 m of where a dredge pipeline was discharging. Depths were 0.5 to 2 m and currents were weak. The dredged material had a median particle size of 4 to 5 μm. Median fluid-mud thicknesses were 0.45 m of which the top 60 percent was interpreted as underflow and the remainder as deposit. Fluid-mud concentration at the upper surface of the underflow layer was about 3 dry-kg/m^3 and increased exponentially with depth to about 48 dry-kg/m^3. The deposit was 48 to 110 dry-kg/m^3 solids.

A numerical model that would simulate underflow fluid-mud spreading resulting from a pipeline discharge was developed as an aid in the diagnosis and interpretation of field measurements. The model was based on one-dimensional equations for momentum and mass conservation. Model features that limited entrainment and concentration change caused by deposition were incorporated as indicated by field observations. A plume of suspended sediment 200 to 500 mg/L above ambient concentration occurred over the underflow footprint, with resuspension driven by wind-waves. The development of a point model of the water column overlying a fluid mud layer was based on a balance between entrainment and settling. Settling was prescribed on the basis of a laboratory-developed functional dependence on concentration. Data were used in the model to estimate coefficients for this entrainment process.

INTRODUCTION: Maintenance dredging of the Gulf Intracoastal Waterway (GIWW) annually involves more sediment than the total of the natural sediment inputs to Laguna Madre (Morton, Nava, and Arhelgar 2001). Hydraulic dredging followed by open-water disposal through a pipeline is the most common dredging method in shallow, vegetated Laguna Madre, TX. There are concerns that redispersed dredged material in Laguna Madre is contributing to turbidity and is limiting light penetration to sea grasses over the long term (Onuf 1994). The extent of initial dredged-material spreading is important information for assessing total resuspension and predicting possible sediment impacts outside designated disposal areas.

Measurements of fluid-mud thickness, concentration structure, and overlying suspension concentration were made north of Port Mansfield, TX, in Laguna Madre, within about 500 m of an ongoing dredged-material pipeline discharge. Such information is scarce, but is needed to improve understanding of the behavior of such discharges and subsequent sediment dispersion. Field measurements were compared here to results taken from a near field, numerical underflow-spreading model for the purpose of improving model formulation. Information was also used to characterize pipeline discharges in a large-scale numerical sediment-transport model of this system (Teeter et al., in preparation). A simple water-column point model was also used to estimate coefficients for an entrainment relationship that would describe the flux of underflow sediment into the water column. As will be shown, the extent of the underflow affects the extent of any surface plume of suspended sediment which might form during or shortly after discharge as a result of entrainment of the underflow into the overlying water column.

The 183-km section of Gulf Intracoastal Waterway (GIWW) in shallow Laguna Madre, TX, is located between Port Isabel and Corpus Christi Bay, or geographic coordinates 26.1° to 27° N, and approximately 97.4° W. This section requires about 1.6×10^6 m^3 of maintenance dredging annually. About 75 percent of the 1,500-km^2 Laguna Madre is vegetated, and seagrasses are sensitive to underwater light conditions (Dunton 1994). A series of studies has recently been undertaken to evaluate the impact of dispersion of sediments from the placement areas on sea grass areas in Laguna Madre (Brown and Kraus 1997; Militello, Kraus, and Kite 1997; Burd and Dunton 2000; Morton, Nava, and Arhelgar 2001; and Teeter et al., in preparation).

BACKGROUND ON PIPELINE DISCHARGE UNDERFLOWS: In shallow water, dredged sediment particles reach the bottom soon after pipeline discharge, settling within a short distance from the discharge point. Sediments form layers of fluid mud at the bed, which flow away from the point of discharge, the extent of the flow depending on bottom slope, ambient currents, and their initial discharge trajectory. Some general characteristics of underflows were presented in TN-DOER-N11 (Teeter 2001).

The approach channel to the Chesapeake and Deleware Canal in Upper Chesapeake Bay was hydraulically dredged in 1988. About 5.2×10^5 m^3 of clayey silt sediment were pumped and deposited in areas D, E, and F near Pooles Island. The movement of sediment was downslope after discharge. A broad continuous layer formed about 3 km long and 1.5 km wide. The maximum deposit thickness was 1.5 m. Sediment consolidated to a density of 1,130 kg/m^3 or greater within several weeks. Dewatering and compaction accounted for 5 percent deposit-volume reduction in 5 months. Another 5 percent reduction occurred during the discharge period. The remaining 22 percent of the 32 percent total reduction was from redistribution by resuspension and transport (Panageotou and Halka 1990).

Near Pooles Island, 5.2×10^5 m^3 were hydraulically dredged from the nearby channel in 1991 and placed in Areas D and E. Sites were 4.5 to 8 m deep. Sediments deposited in a natural trough and constructed trenches. The sediment remained in the deep, trough area. The volume of the deposit was 1.04×10^6 m^3 with maximum thickness of 3 m. Sediment were clayey silt with minor sand. Bulking factor between in-place and deposited volumes was about 1.75. One year later the deposit was 4.4×10^5 m^3 (58 percent reduction). Four-fifths of the reduction was attributed to dewatering, one-fifth to erosion (Panageotou and Halka 1994).

FIELD OBSERVATIONS: Field experiments were carried out to take advantage of dredging conducted in February 2000 to remove a 1.8-m layer of material deposited in the GIWW as a result of a hurricane the previous year. Dredge *J.N. Fisher* discharged into open-water disposal sites through a 50.8-cm-diam pipeline, using a 1,500-kW (2,000-hp) pump. The dredging rate was about 1,100 m^3/hr, and, based on the solids content of the channel material, the sediment discharge rate was about 50 dry-kg/sec.

Fluid-mud thicknesses, or heights, and densities were measured on 2 days while pipeline discharge was occurring. Locations for the discharges are shown in Figure 1. A special push-tube sampler allowed for fluid-mud density determination within only a few minutes of sampling. Samples were collected for analysis of the fluid-mud concentration to supplement the field-density measurements. Fluid-mud particle-size distribution and ambient water column suspended-sediment concentrations were also measured. A composite sample was used in the laboratory to determine velocities in the hindered settling range.

Field Methods. A 5.8-m-long flat-bottomed boat with a propeller tunnel to minimize draft was used for sampling. A Starlink ® Differential Global Positioning System was used to locate stations to within ±2 m, and an HP PalmPC ® was used to log positions in the field. Water-column samples were collected with a submersible Rule ® electric pump and 1.5-cm-diam hose. Water samples were collected at middepth and 0.3-m depth and stored in 225-ml plastic bottles.

Fluid mud was sampled with a push corer with a clear 3.6-cm-diam core tube and a total length of about 3 m. During the first sampling day, it was found that the in-line check-valve developed too much back pressure, resulting in significant errors in underflow sampling. For the second sampling day, fluid-mud samples were collected with a low back-pressure push-core sampler specially fabricated from parts of a WILDCO ® corer. That sampler can be seen in Figure 2. Only the fluid mud measurements from the second day are reported.

The boat was brought to a new location, and the anchor was set. A couple of minutes were allowed for the boat to swing to and for the position to be logged. The corer was pushed vertically downward by hand until it encountered firm bottom. A trip line was then pulled to seal the top of the sampling tube. The corer captured ambient water column, fluid mud (if present), and a short plug of the underlying bottom material. (The bottom material contained an appreciable sand fraction not present in the dredged material and had a bulk density of roughly 1,500 kg/m^3). The vertical alignment of the core tube was maintained as it was lifted to the deck and a piston push-rod was inserted into the lower end of the core tube (below the sediment plug). After the core tube was unscrewed from the remainder of the sampler, the piston rod was pushed upward to expel the sample from the end of the tube. By incrementally extruding the sample from the end of the core tube, scientists could take measurements and subsamples over the vertical dimension of the fluid mud. Density measurements were made in the field with a PARR ® DMA35 vibrating-tube densitometer (precision of 1 kg/m^3). A short length of 2-mm-diam tubing was inserted 2.5 cm into the end of the core tube, and a 5 to 10 cm^3 sample was drawn through the densitometer. Field density measurements were made in duplicate and averaged.

Laboratory Methods. Laboratory bulk wet density determinations were made with the use of 25-cm^3 wide-mouth pycnometers. Pycnometers were weighed after being mostly filled with sample

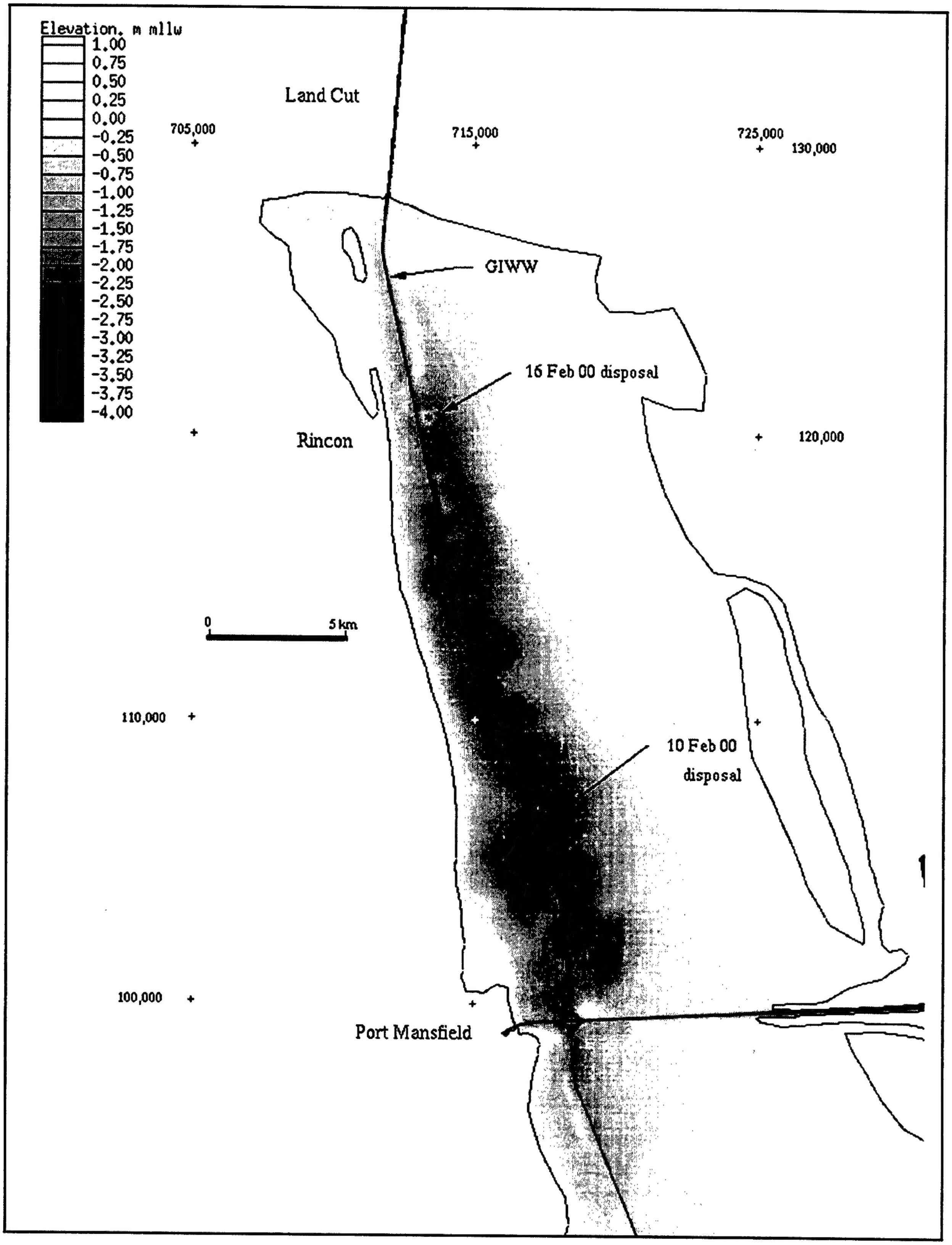

Figure 1. Vicinity sketch of Lower Laguna Madre north of Port Manfield, TX, with depth contours and discharge locations (coordinates are State Plane NAD27, Texas South, in meters)

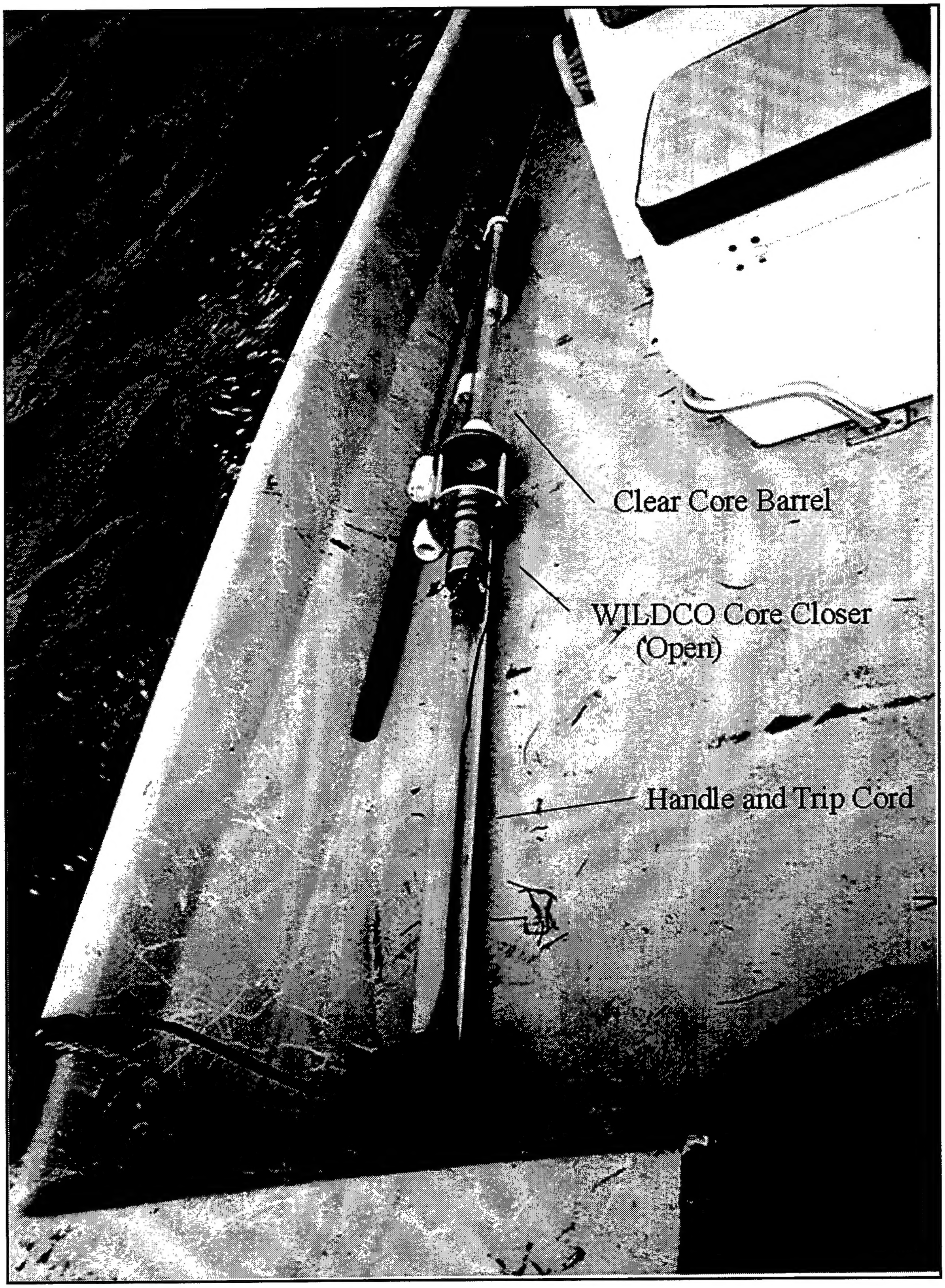

Figure 2. Fluid mud sampler on deck in open position

and then carefully topped with distilled water. Bulk wet density was calculated from this information and known characteristics of the pycnometers. Pore-fluid density was estimated on the basis of the salinity determined on suspended samples, allowing the calculation of sample solids content from bulk wet density (assuming a solids density of 2,650 kg/m^3).

Total suspended material (TSM) was determined by a gravimetric method for nonfilterable solids with preweighted Nuclepore ® 0.45 µm pore diam, polycarbonate filters. After being used to filter a known volume, filters were rinsed with distilled water, and dried 1 hr at 90 °C and then reweighed. Particle-size distribution was measured with a Coulter LS100Q ® laser scattering instrument. Samples were first oxidized with Clorox ® to remove organics and then were dispersed with sodium carbonate/bicarbonate. Three oxidation steps and three dispersion steps were performed before samples were processed through the Coulter instrument to determine particle size. The Coulter has 128 geometrically spaced channels, or bins, for sizing.

Settling velocities in the hindered-settling concentration range were measured on left-over sample that had been composited to make a slurry. The slurry had a bulk density of 1,109.5 kg/m^3, pore-fluid density of 1,025.7 kg/m^3 (37.3 ppt), and solids content of 136.7 dry-kg/m^3. Sample was incrementally added to a 2-L glass, graduated cylinder which was 7.74 cm in diam and 42.5 cm high at the 2-L level. Six tests with concentrations of 6.8 to 66.3 dry-kg/m^3 were made at 23 °C. After the sample was mixed in the cylinder, height of the interface between the suspension and the clear layer that formed was observed over time. The duration of the lowest initial-concentration test was about 1 hr. During other tests, frequent measurements were collected over 100 to 240 min; these tests lasted a total of 1,100 to 1,450 min. Final data points allowed for estimation of average density after about 1 day of settling time.

Linear regressions were fit to the data for the period when the interface descended linearly (n = 3 to 20, R^2 = 0.944 to 0.999, standard error on slope = 1.82 to 0.025 mm/min) to determine the hindered settling velocity (W_s) at initial test concentration C. Tests with the lowest two concentrations were repeated, and data sets were combined in the regression analysis. Finally, W_s and initial concentration from the six tests were combined and fit to an empirical equation for hindered settling dependence on concentration:

$$W_s = Wh_o (1 - k\,C)^n \;, \quad C > \text{hindered-settling threshold} \tag{1}$$

where the hindered settling threshold is usually in the range of 1 to 10 dry-kg/m^3.

Field and Laboratory Results. All settling tests were in the hindered settling concentration range. Settling rates decreased about two orders of magnitude over the concentration range tested. Data greater than 6.8 dry-kg/m^3 fit Equation 1 well with the reference hindered settling velocity Wh_o = 0.5 mm/sec, coefficient k = 0.005 m^3/kg, and the exponent n = 11. Settling test results are plotted in Figure 3 along with results from the low-concentration settling tests performed by Teeter et al. (in preparation), using Laguna Madre GIWW sediments collected about 3 km north of Port Isabel. The mean depth-average concentration at the end of the settling tests (about 20 hr) was 115.5 dry-kg/m^3 (with one high outlier of 148 dry-kg/m^3 removed, n = 4, 95 percent confidence interval 112.0 to 118.9 dry-kg/m^3).

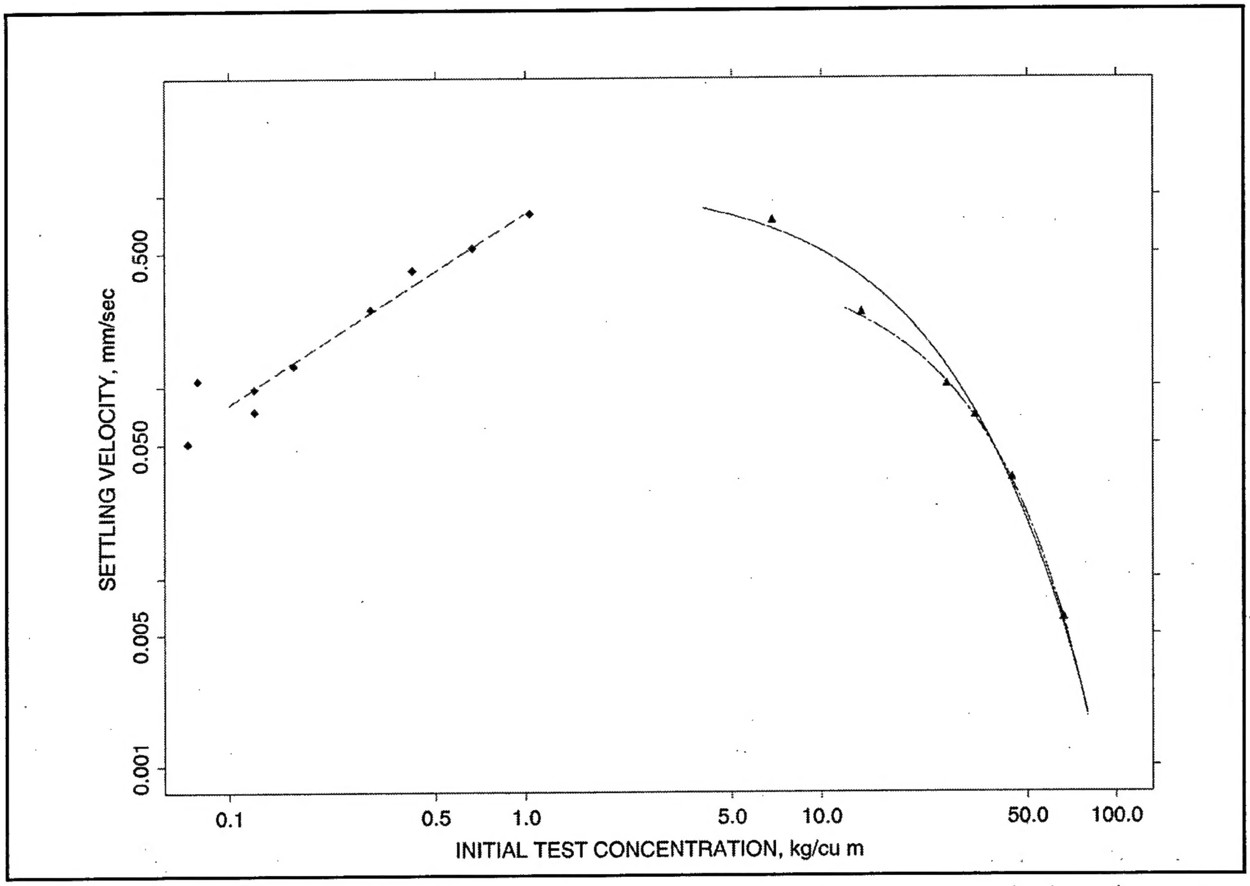

Figure 3. Hindered settling test results (right) with the (dashed) fit to the data described in the text, and low-concentration settling results (left) from Teeter et al. (in preparation)

February 10. When sampling began at 1000 Central Standard Time (CST) on 10 February, south winds were 9 m/sec, making sampling conditions difficult. Currents were weak and toward the south. The pipeline discharge was located at coordinates 26° 37.4358' N and 97° 24.8643' W, about 3.7 km north of the entrance to Port Mansfield at the disposal area designated PA 218 (Figure 1). A plot of the station locations, CST, and depths in a local horizontal coordinate system are shown in Figure 4. The pipeline was located 20 m west of the 1016 CST station and changed only slightly as the dredge moved. Water-column samples taken at 0.3 m depth had TSM levels (mean = 211 mg/L, 95 percent confidence interval 51 to 370 mg/L, n = 12) equivalent to those from middepth (mean = 199 mg/L, 95 percent confidence internal 55 to 344 mg/L, n = 11). Both sampling depths showed highly variable TSM. Depth-averaged TSM are shown in Figure 5. High-suspension concentrations were measured both north and south of the pipeline discharge. Depth-average TSM values of 549, 557 and 572 mg/L were obtained near and downdrift within about 660 m of the discharge. Stations taken at 1107, 1126, and 1255 CST had what was apparently background level TSM ranging from about 100 to 120 mg/L. One station (1200 CST) taken upstream of the discharge had 262 mg/L TSM, possibly as the result of local resuspension.

A photograph taken from 1,900-m altitude above the dredging operation at 1019 CST is shown in Figure 6. The pipeline length was about 450 m, and the discharge flowed to the east of the channel. Ambient and dredged-material plumes at both the dredging and disposal sites are shown in the

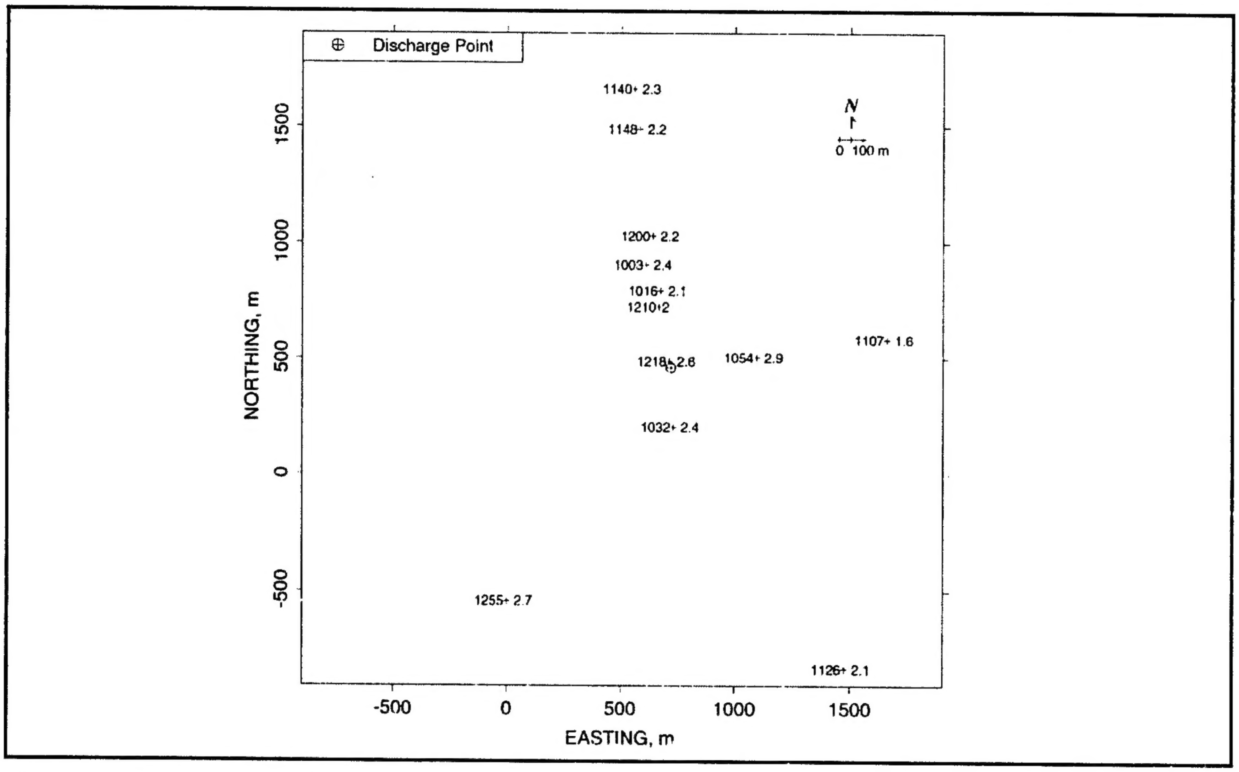

Figure 4. Times/depths (CST/m) for stations taken 10 February 2000

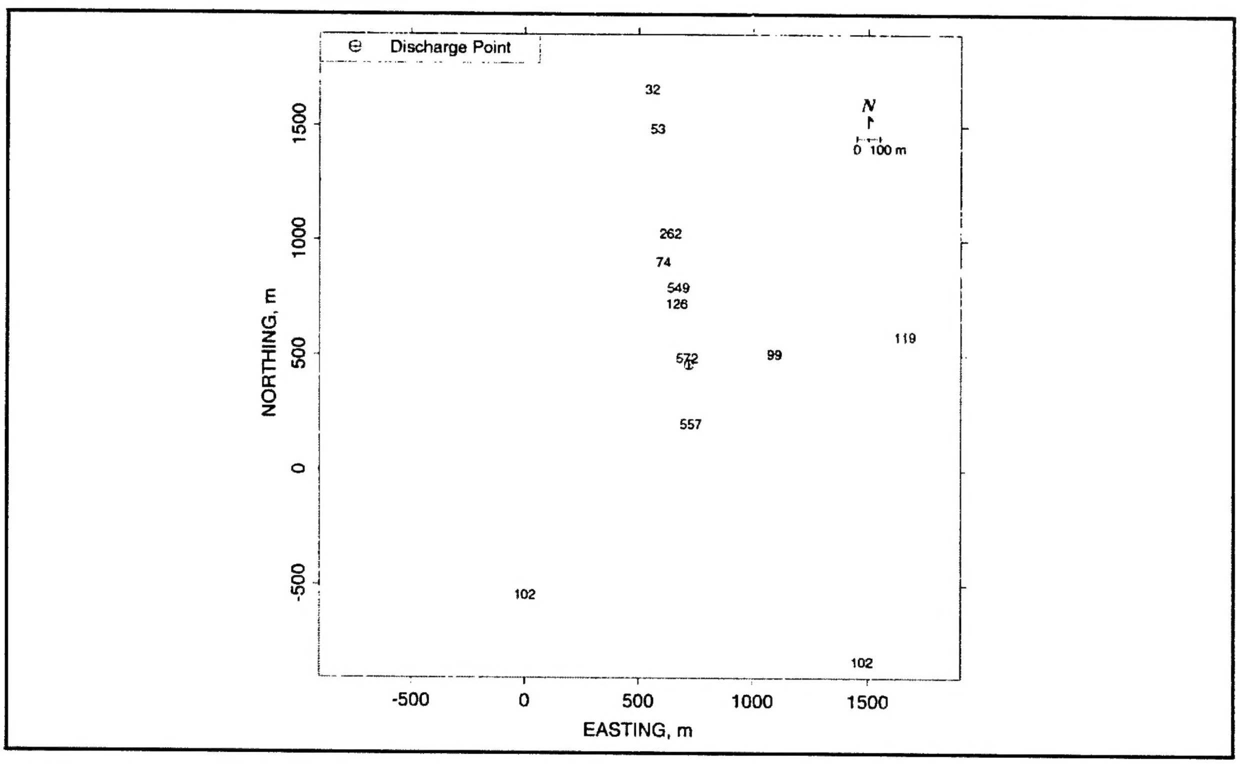

Figure 5. Depth-averaged TSM (mg/L) collected 10 February 2000

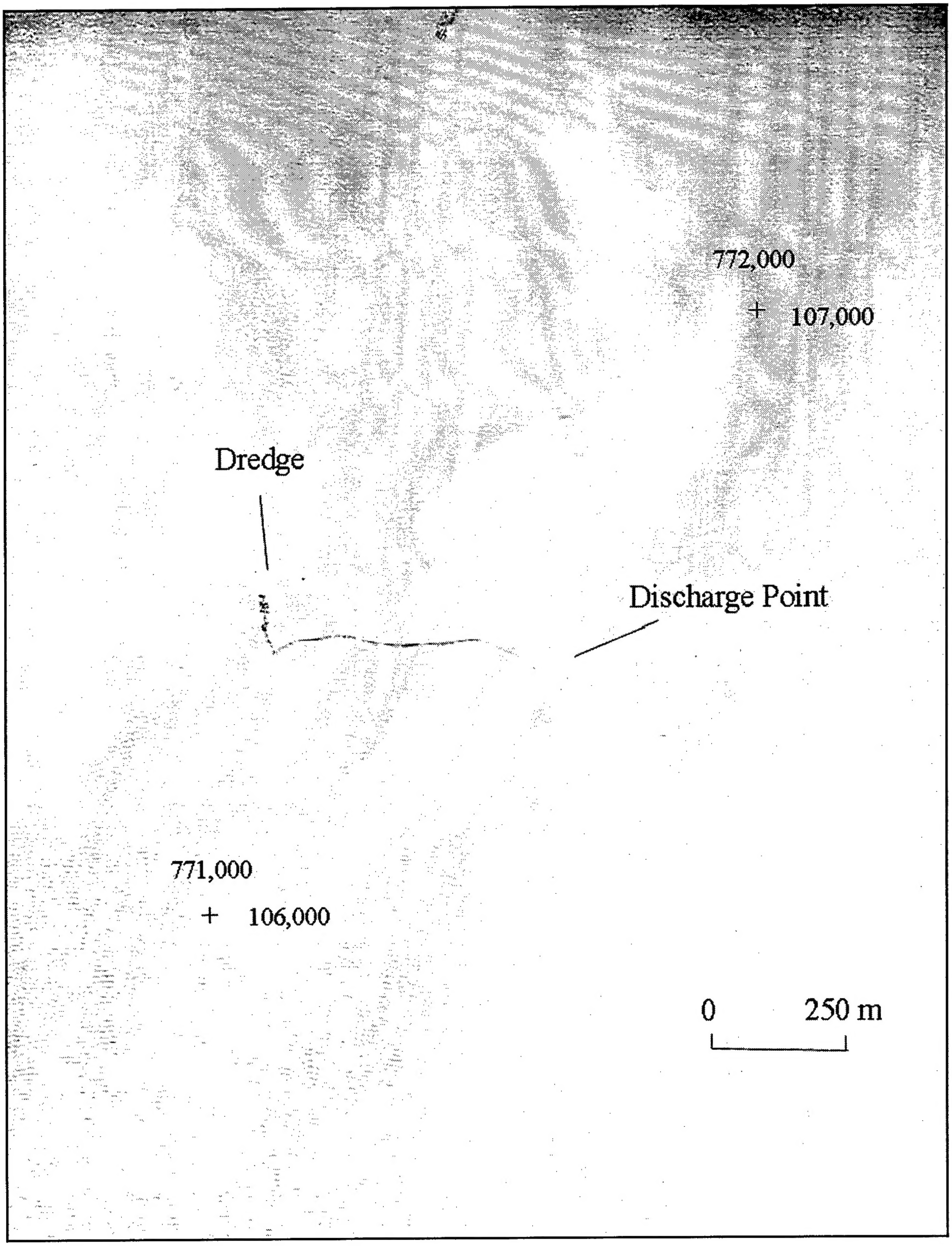

Figure 6. Overflight photo of dredging and disposal operation taken 1019 CST 10 February 2000 (coordinates are State Plane NAD27, Texas South, in meters)

photograph. The aerial photograph shows the area directly south of the discharge to be the heaviest visible plume. A plume emanating directly from the discharge had a blue coloration, while other plume areas were milky.

February 16. Winds were from the south. Waves were 0.30 cm or less. Currents were weak and moved toward the north (≈2 cm/sec). The pipeline discharge was located at coordinates 26° 44.9752' N and 97° 27.3349' W, about 3.3 km south of the entrance to the Land Cut, at PA 213 (Figure 1). The discharge was to the east of the channel onto a mound with about a 0.3-m water depth. Dredging records indicated that the previous discharge location was 360 m north in PA 213. Discharge started there at about 2200 CST on 15 February; the discharge that was sampled began at about 0800 CST on 16 February. During the sampling period, 12,000 to 15,000 m^3 of dredged material was discharged at these two sites.

Station times and depths are shown in Figure 7. A turbulent surface flow formed in the vicinity of the discharge jet and extended into deeper water. A photograph of the surface jet and flow is shown in Figure 8. A plunge line could be clearly seen in the field at a water depth of about 1 m, and an underflow moved toward the deeper water to the east-southeast. Samples taken at 0915 CST were within the turbulent surface flow, and two field measurements and two pump samples indicated that the turbulent surface flow averaged 17 dry-kg/m^3.

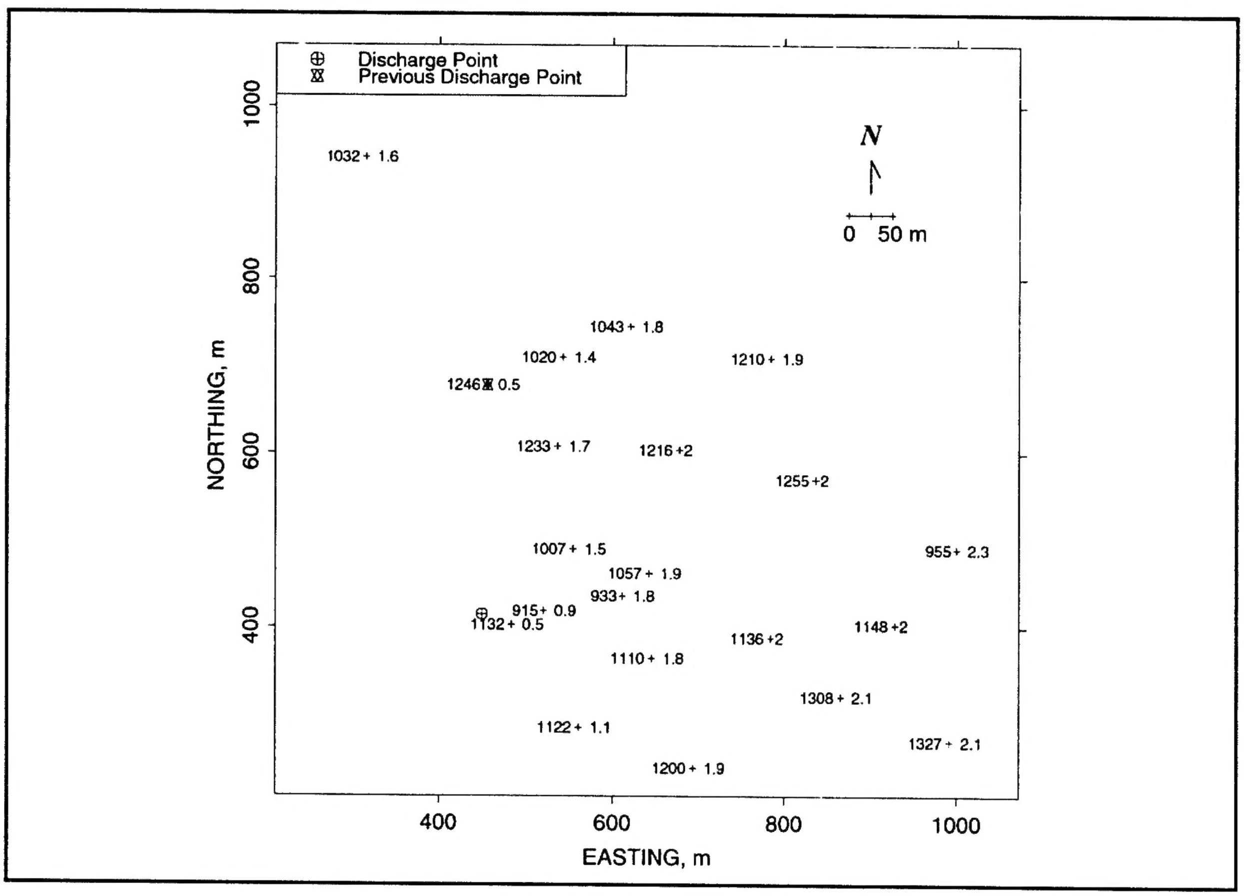

Figure 7. Times/depths (CST/m) for stations taken 16 February 2000

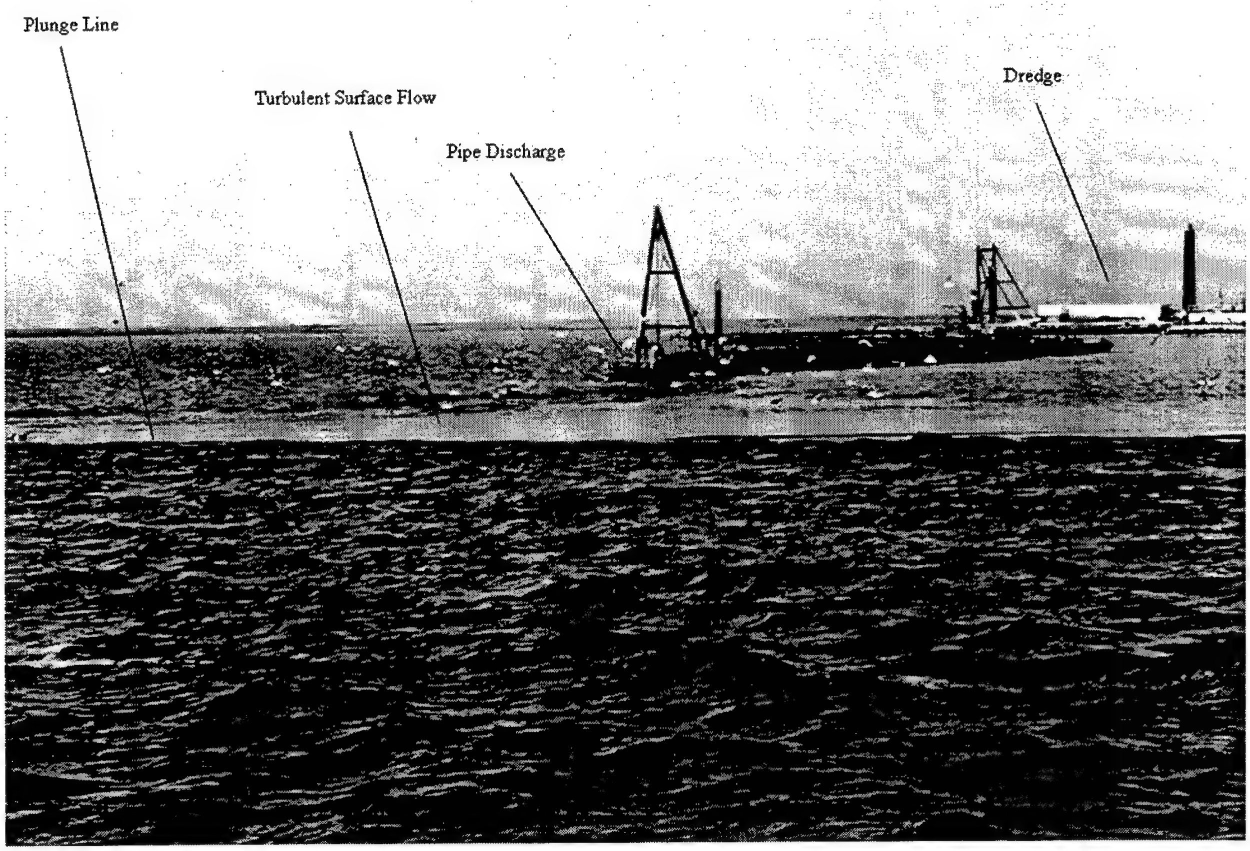

Figure 8. Pipeline discharge into approximately 0.5-m water depth and resulting turbulent surface flow

Fluid mud formed a sharp interface with the ambient suspension, and its thickness was easily measured through the clear 3.6-cm-diam core tube. Fluid-mud profiles are presented in Figure 9. Because of concerns about settling effects and time constraints, few samples near the upper underflow interface were made. The fluid-mud layer was highly stratified in the vertical. Gradients indicated that concentrations at the upper interface were low. Several measurements indicated minimum underflow concentrations of 3 to 5 dry-kg/m^3. However, the upper surface of the underflow was a distinct, sharp interface, indicating a concentration jump associated with the maximum flux of suspended material (Teeter 1986). Concentrations in the underflow were therefore above the concentration at which the maximum settling flux occurred. The maximum settling flux apparently occurred between the settling flux at 6.8 dry-kg/m^3 (0.0051 kg/m^2/sec) determined in the hindered settling tests and the previous 1 dry-kg/m^3 low-concentration test (0.0006 kg/m^2/sec). Thus, 3 dry-kg/m^3 was estimated to be the minimum or underflow interface concentration. Points were added to profiles as shown in Figure 9 at the measured interface locations and the assumed 3 dry-kg/m^3.

Fluid-mud layers consisted of underflow and deposit, as interpreted by the following information. Near the top of the fluid-mud layers, concentrations increased exponentially with depth and in approximately straight lines when plotted on semi-log axes as in Figure 9. This distribution would be expected for a turbulent flow with a particle Peclet number ($Pe = W_s h/K_z$ where h is the underflow

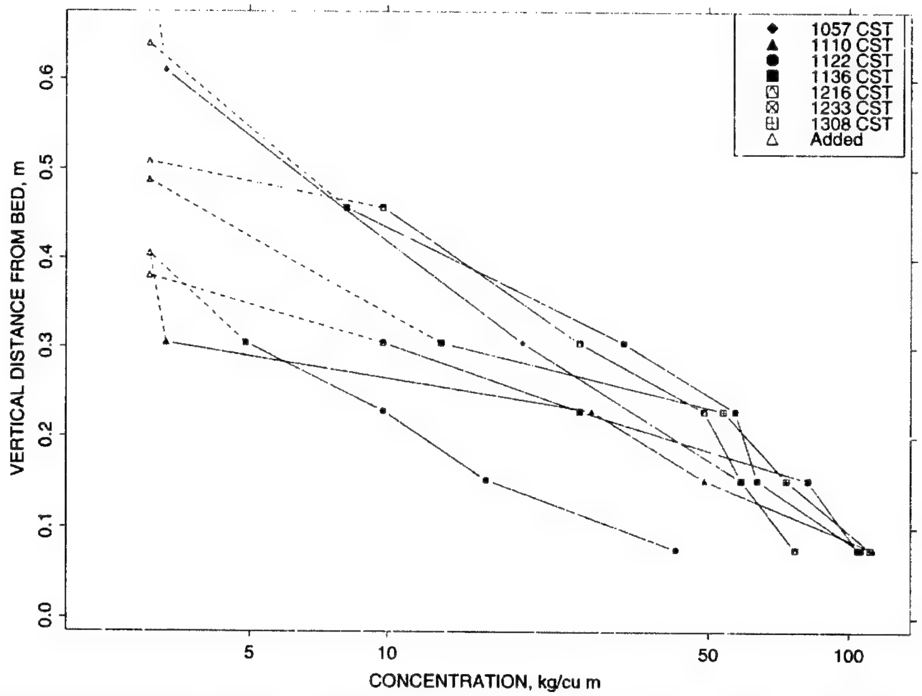

Figure 9. Vertical fluid mud profiles taken 16 February 2000

thickness and K_z is the layer-average turbulent diffusivity) greater than about one (Teeter 1986). Another steeper gradient was evident below many of these exponential layers, and, taking all measurements together, the statistical distribution of fluid-mud concentrations had an inflection at about 50 dry-kg/m^3. Previous laboratory experiments on sediment from nearby Corpus Christi Bay (76 percent clay and 21 percent silt) indicated that the mean concentration of newly-deposited material was 46 dry-kg/m^3 (Teeter 1986). Therefore, the lower portion of these fluid-mud layers was interpreted as deposit from the underflow, while the upper layer, with concentrations of about 3 to 48 dry-kg/m^3, was interpreted as the underflow. Normalized underflow concentration profiles were similar, as can be seen in Figure 10, and their exponential shapes suggest some degree of vertical mixing, consistent with a flow with some turbulence.

All measured fluid-mud thicknesses and a rough interpretation of the underflow footprint extent are shown in Figure 11. The 0915 CST samples were assigned 0.0 fluid-mud thickness in this figure because they were located within the turbulent surface flow. It appeared that the underflow footprint formed by the discharge ongoing during sampling overlapped that formed at the previous discharge location. Underflow mean concentrations C, thickness h, and deposit thickness *delbed* were calculated on the basis of a 50-point interpolation over the fluid-mud profiles as shown in Figure 12 for these stations, along with the water column depth above the underflow (H_o).

Surface TSM levels (mean = 258 mg/L, 95 percent confidence interval 114 to 402 mg/L, n = 17) and middepth levels (mean = 262 mg/L, 95 percent confidence interval -205 to 728 mg/L, n = 8) were equivalent again this day. A plot of depth-mean TSM values is shown in Figure 13, along with an interpreted underflow footprint extent. As can be seen, the highest suspended concentrations

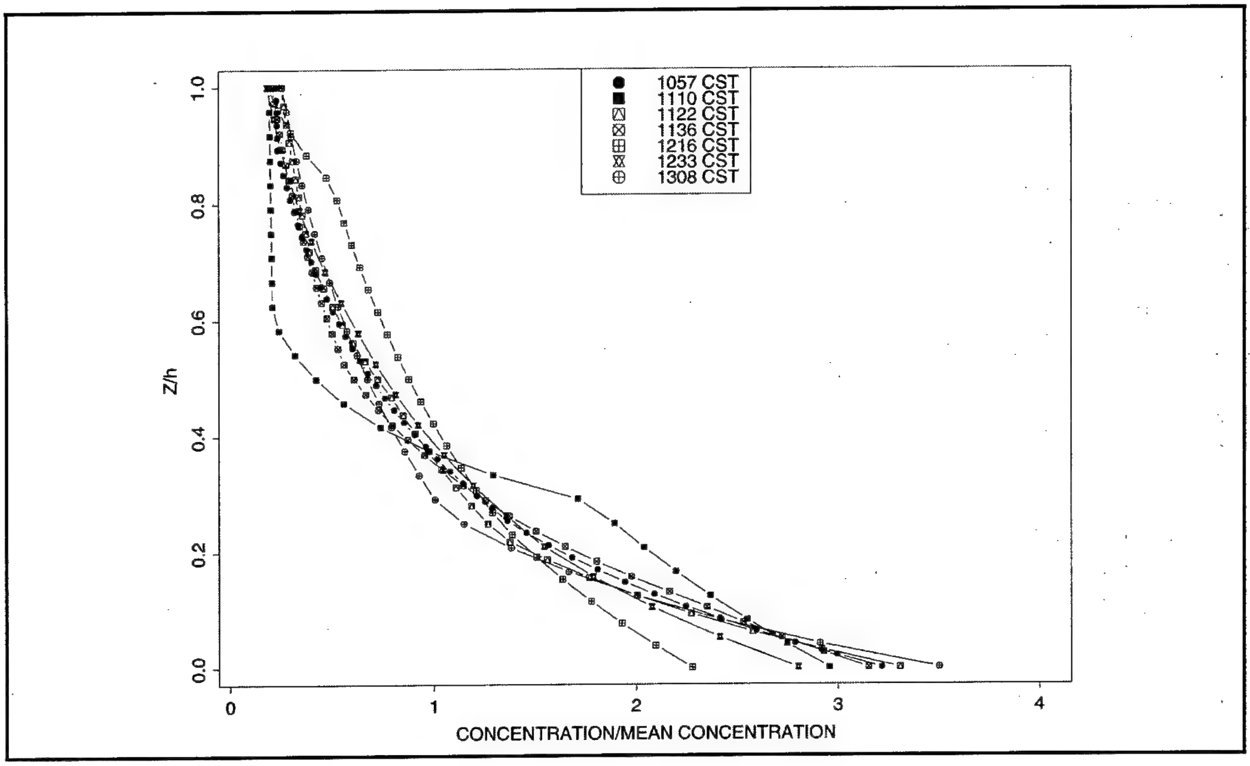

Figure 10. Interpreted and interpolated underflow profiles normalized by underflow thicknesses and mean concentrations

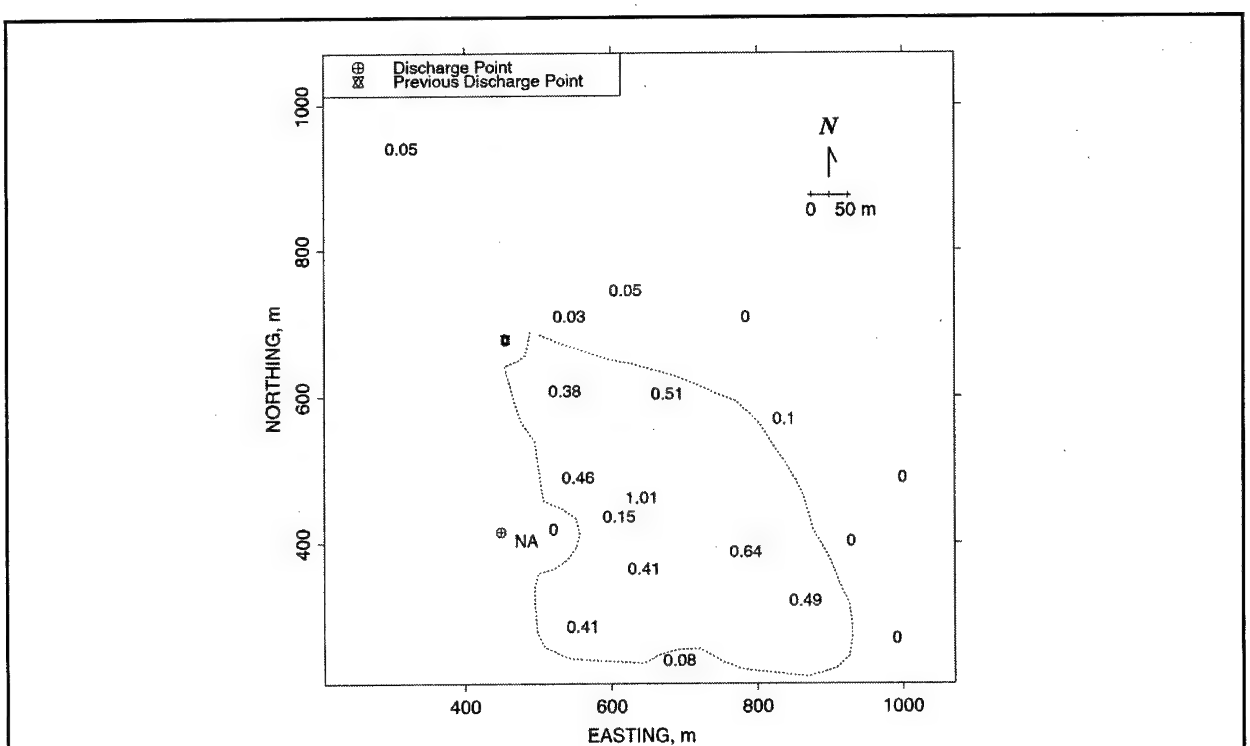

Figure 11. Fluid mud thicknesses collected 16 February 2000

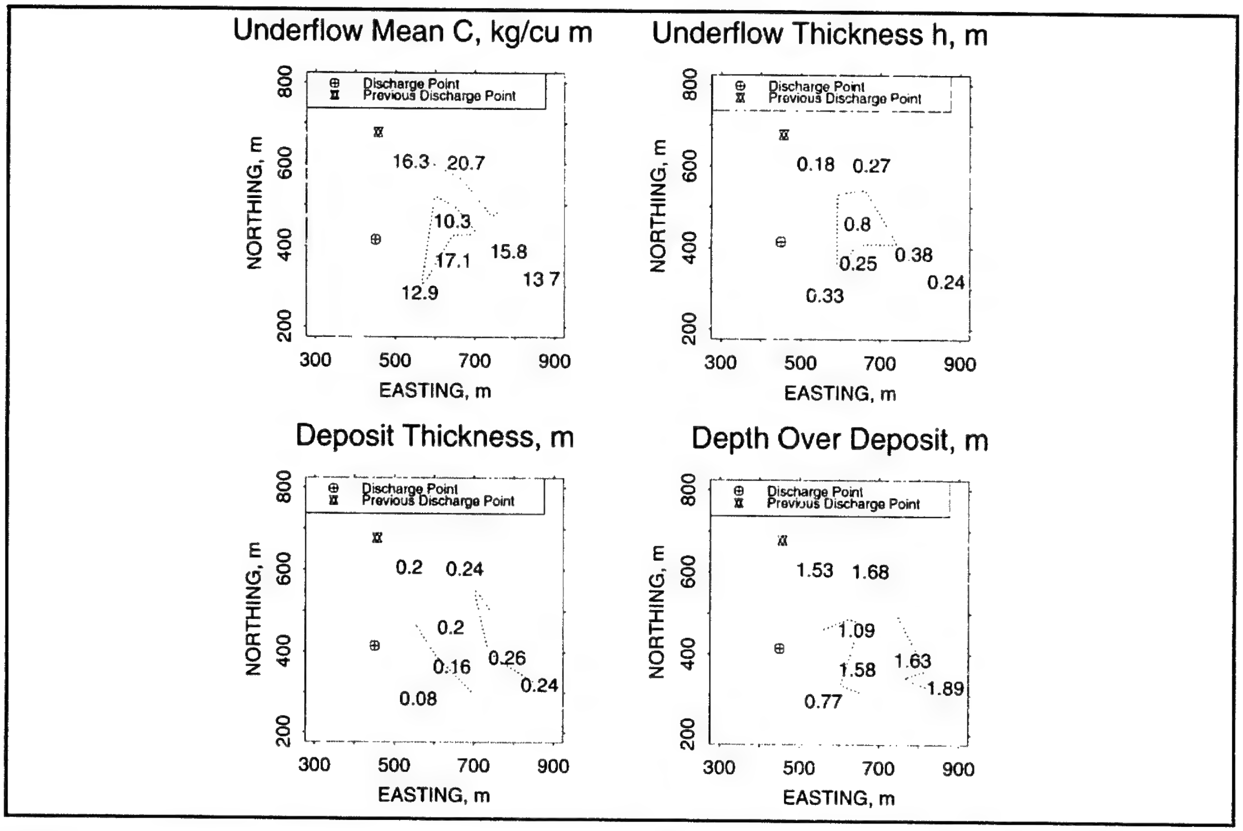

Figure 12. Interpolated underflow mean concentrations, thicknesses, deposit thickness, and water column depth over underflow for mud profile stations, 16 February 2000

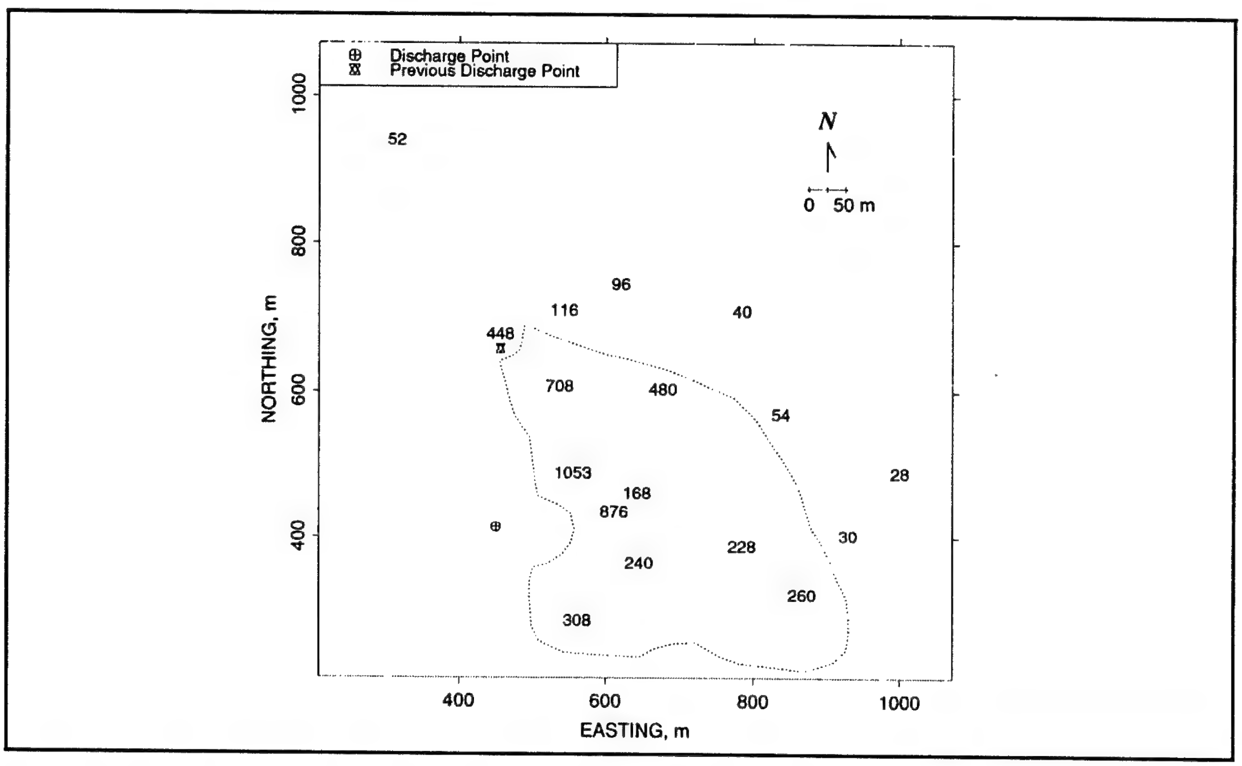

Figure 13. Depth-averaged TSM (mg/L) collected 16 February 2000

occurred over the underflow, whether upstream or downstream from the discharge point. The implication is that wind-waves were acting to entrain material from the active underflow and from the previous underflow into the water column. Since water-column advection was minimal, the resulting TSM plume did not appear to extend much beyond the footprint extent (and vice versa).

Comparisons between field measurements and laboratory densities indicated that many field samples had sampling errors and were biased toward lower density. These samples took much longer to obtain than the field density measurements did, and settling may have caused the bias. Results from the field densitometer and pycnometers agreed well on samples tested in the laboratory. Therefore, density results from samples were not included in previous figures. Table 1 summarizes laboratory analyses of particle-size characteristics on fluid-mud point samples. In that table, H is water depth to the original bed, z_i is the distance up from the bottom, and D_{50} is the median dispersed grain diameter.

Table 1
Summary of Fluid-Mud Sediment Characteristics from Near Pipeline Discharge

Time, CST	H, m	z_i, m	D_{50}, µm	% <4 µm	% <16 µm
915	0.9	0.6	4.4	47	84
915	0.9	0-0.15	5.1	43	79
933	1.8	0-0.15	5.1	43	78
1007	1.5	0.15	4.2	49	86
1007	1.5	0-0.15	4.1	50	85
1057	1.9	0.3	3.9	50	87
1057	1.9	0-0.15	4.3	49	84
1110	1.8	0-0.15	4.4	47	85
1122	1.1	0-0.15	4.2	49	86
1136	2	0-0.15	4.1	49	86
1216	2	0-0.15	4.1	50	86
1233	1.7	0-0.15	4	50	88
1308	2.1	0-0.15	4.2	50	86

UNDERFLOW SPREADING PROCESSES: To better understand the spreading of the fluid-mud underflow, a mathematical description of underflow processes was developed. Unfortunately, there are no analytic solutions for the case of a particle-driven gravity flow which is entraining and depositing material, so a numerical solution was developed. Important model features were guided by field observations with special attention to entrainment and settling, either of which can appreciably reduce underflow concentration.

Model Description. A model was constructed to compute total flow or discharge (Q), sediment flux (CQ), breadth (B), and height (h) along the length (x) of an underflow by numerically integrating a set of governing equations downslope in the direction of the underflow. The development of both model equations and assumptions were guided by the field observations. The behavior of mobile

fluid-mud layers is an active area of research, and more studies will be needed before such computations can be made with confidence.

The bed was assumed to be planar with an arbitrary slope which was allowed to vary in the downslope direction. The underflow was considered quasisteady or steady over a short duration of time. Thus, time derivatives were ignored in the governing equations. However, time of travel to every discrete location along the underflow trajectory was calculated by integrating the underflow velocity. After the first full numerical integration sweep from the transition (beginning) to the end of the underflow, subsequent sweeps were made at discrete time intervals and included updated bed elevations based on the cumulative deposit thickness from preceding sweeps. Sweeps were made at intervals of 1,800 sec so that per-sweep deposit-thickness changes were small. Thus, the model made many sweeps over the underflow domain and duration of the discharge to update deposit thickness *delbed* and bed slope. Other variables were calculated from the basic state variables and used to solve auxiliary equations for entrainment, bed friction coefficient, depositional flux, and lateral spreading. These variables include underflow concentration (C), velocity (U), deposit thickness, Reynolds and Richardson numbers.

Equations. Governing layer-averaged equations are based on mass and momentum conservation. Governing equations for steady, one-dimensional gravity flow momentum have been developed by Ellison and Turner (1959), Parker, Fukushima, and Pantin (1986), and Van Kessel and Kranenburg (1996). Ellison and Turner (1959) ignored $\Delta\rho/\rho_l$ terms except when combined with g where g = the acceleration of gravity, $\Delta\rho$ = the density difference between the underflow and the overlying ambient suspension (i.e., $\rho - \rho_l$ where ρ_l = constant), ρ = the layer density ($\rho = \rho_l + \Delta\rho$). This is equivalent to ignoring them in inertia terms of the equations of motion, and thus the fluid is treated as having uniform mass, variable weight, and conservative buoyancy. Parker, Fukushima, and Pantin (1986) derived equations explicitly for particle-driven gravity currents where deposition and erosion can occur and can affect layer buoyancy. They began with the three-dimensional Navier-Stokes equation. However, they also assume uniform mass density. Van Kessel and Kranenburg (1996) cite Ellision and Turner (1959) as developers of an appropriate layer-averaged integral momentum equation but made a key change by keeping the density term inside the momentum derivative. In this way mass density and mass flux are not assumed constant in the x-direction. The following paragraphs derive a form of their equation for a wide, variable-width flow of rectangular cross section.

The momentum equation was developed considering the forces acting on the boundaries of an elemental flow volume. Some definitions are given in Figure 14. The momentum of a flow volume with width B between x and $x + dx$ and planes normal to the x-axis and parallel to the z-axis is the mass times its velocity. Let ρ be density of the flow. Then $\rho Bu\,dt$ is the mass passing through the upstream plane per unit depth, where u is the mean flow across the plane. Since the mass moves at u, the time-averaged momentum is ρBu^2 per unit depth.

Consider the forces acting on the boundaries of the flow volume. They include the pressure forces (in excess of the hydrostatic pressure) acting on the downstream and upstream planes, reactive shear-stresses acting along the bottom and the top ($\tau_b + \tau_t = \tau$ where = bed shear stress, τ_t = shear

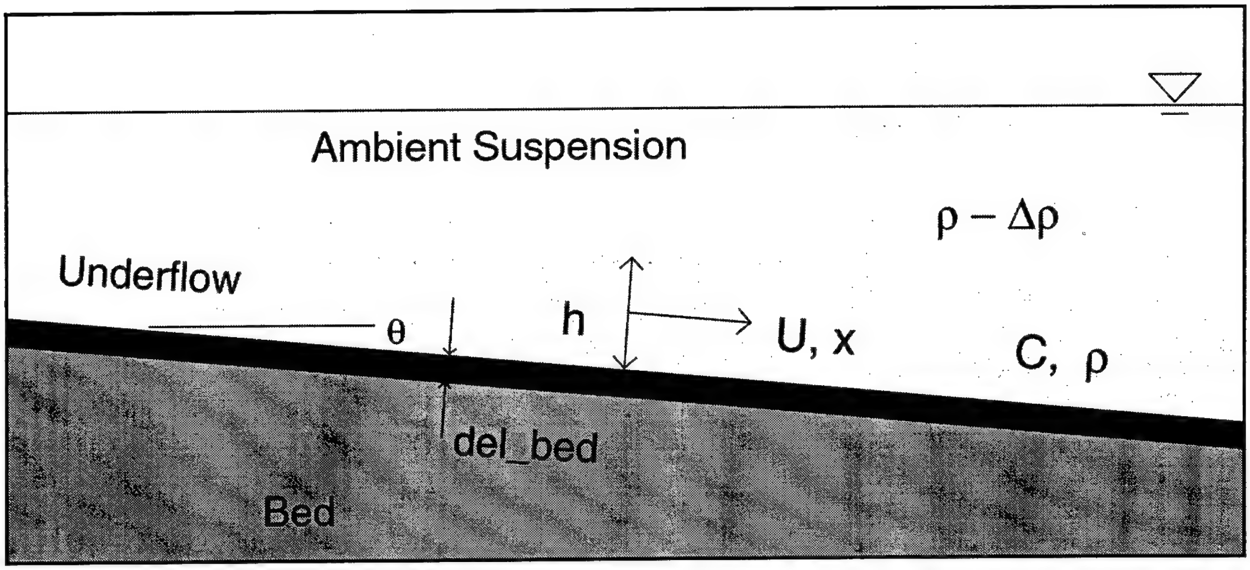

Figure 14. Definitions for some model variables

stress at the top of the underflow, and τ is the total) , and a body-force accelerating the volume downslope. Then the momentum balance is

$$\frac{d}{dx}\int \rho\, B u^2\, dz = -B\tau - g\cos\Theta \frac{d}{dx}\int \Delta B z\, dz + g\sin\Theta \int \Delta\rho\, B dz \tag{2}$$

where the left-hand side term is the change in momentum along the slope, and the right-hand side terms are (a) the total shear stress resisting the flow; (b) the derivative of the pressure along the flow resulting from changing depth and density; and (c) the gravity force acting to accelerate the layer.

Assume $h(x)$, $\Delta\rho(x)$, $B(x)$, and $U(x)$ vary along the flow. Define variables for mass and momentum: $\rho BUh = \int \rho Bu\, dz$ and $\rho BU^2 h = \int \rho Bu^2\, dz$. Shape factors $S_{1,2}$ are defined during integration of pressure and gravity terms taking into account z-direction variations in density $\rho(x)$ such that

$$\begin{aligned} S_1\, \Delta\rho\, Bh^2/2 &= \int \Delta\rho\, Bz\, dz \\ S_2\, \Delta\rho\, Bh &= \int \Delta\rho\, B dz \end{aligned} \tag{3a,b}$$

The excess density is integrated and the hydrostatic pressure does not appear. Thus, vertical integration is done under the assumption that shape factors do not vary in the x-direction. The momentum equation is then cast as

$$\frac{d\left(\rho BU^2 h\right)}{dx} = -B\tau - \frac{S_1 g\cos\Theta}{2}\frac{d\left(\Delta\rho\, Bh^2\right)}{dx} + S_2 g\,\Delta\rho\, Bh\sin\Theta \tag{4}$$

where Θ = the angle of the bed from the horizontal.

Van Kessel and Kranenburg (1996) assumed the shape factors were unity for laminar flow and used a form of Equation 4 with $B \equiv 1$ to analyze turbulent flows. Parker, Fukushima, and Pantin (1986) evaluated shape factors using experimental data and found the top hat assumption for all vertical profiles (including momentum) to be a good approximation. Ellison and Turner (1959) found $S_1 \approx 0.2$ to 0.3 and $S_2 \approx 0.6$ to 0.9 in their experiments. Density profiles from Laguna Madre were integrated after exponential interpolation at 1-cm increments between measurement points ($n = 19$ to 47). Profiles are shown in Figure 9 and dimensionless profiles are shown in Figure 10. The trapezoidal integration of Equation 3 yielded $S_1 \approx 0.58$ ($n = 7$, 95 percent confidence interval 0.53 to 0.64) and $S_2 \approx 1.0$. The shape factors are hereafter assumed equal to unity and omitted from the equations that follow.

The conservation of sediment flux in the flow is

$$\frac{d(CQ)}{dx} = -BS \tag{5}$$

where S = the depositional flux. To adjust the discharge to include entrainment and deposition, such that deposition does not decrease concentration, the conservation of underflow volume becomes

$$\frac{dQ}{dx} = B\left(E_w U - S/C_s - PW_s\right) \tag{6}$$

where E_w = the entrainment coefficient, C_s is the deposit solids content, and P is the depositional probability. The first term in parentheses on the right side of Equation 6 increases underflow volume due to entrainment. The second term decreases flow due to deposition. This term includes both solid and liquid phases of the deposit. The third term in parentheses decreases volume due to liquid leaving through the top of the underflow and is several times larger than the deposit volume rate of change. The underflow is not an irreversibly-mixed solution but rather a settling suspension. By the inclusion of the second and third right-hand term, Equation 6 is different from equations used in other models of particle-laden gravity currents and was developed under the assumption that the fluid mud layer collapses onto the bed during deposition. Thus, deposition decreases Q (and CQ) but does not decrease underflow C in the model.

Wolanski et al. (1992) showed that very low levels of turbulence decrease W_s in the hindered settling concentration range by factors of 2 to 10. This is the justification for the inclusion of the depositional probability P in Equation 6.

Equation 4 can be manipulated to give the thickness change along x caused by momentum:

$$\frac{dh}{dx} = h\left[\frac{1.43C_f}{h} - \frac{Ri\tan\Theta}{h} + \left(\frac{Ri}{2} - \frac{\Delta\rho}{\rho}\right)\frac{dQ}{Qdx} + \left(\frac{Ri}{2} - \frac{\Delta\rho}{\rho}\right)\frac{d(CQ)}{CQdx} + \left(\frac{Ri}{2} - 1\right)\frac{dB}{Bdx}\right] \Big/ (1 - Ri) \tag{7}$$

where C_f = a drag coefficient, the factor 1.43 relates the bed shear stress to the total of the bed and the top shear stresses (Findikakis and Law 1998), and the bulk Richardson number for the flow is

$$Ri = \frac{g\,\Delta\rho\, h \cos\Theta}{\rho\, U^2} \tag{8}$$

The excess density $\Delta\rho$ is related to the underflow concentration $C: \Delta\rho = s'C$ where $s' = (\rho_s - \rho_1)/\rho_s$ and ρ_s = the sediment particle density.

Deposition. The depositional flux is $S = PW_sC_b$, where the probability of deposition $P = 1 - \tau_b/\tau_{cd}$, τ_{cd} = the threshold shear stress for deposition, and C_b = the concentration at the interface with the deposited bed. Deposition does not occur at bed shear stresses greater than τ_{cd}. Since the underflow was found to be highly stratified with respect to C, an expression from Teeter (1986) was used to estimate C_b:

$$C_b = C\left(1 + \frac{Pe}{1.25 + 4.75\,P^{2.5}}\right) \tag{9}$$

where $Pe = W_sh/K_z$ is a particle Peclet number, and $K_z = 0.067(\tau_b/\rho)^{1/2}h$ is taken as the layer-average diffusivity. The valid range for Equation 9 is limited, and the value of C_b/C_o is assumed to have a maximum of 4. Since underflow concentrations are in the hindered range, Equation 7 decreased the depositional flux relative to that calculated with use of the mean concentration.

Flow regime. A Reynolds number (R) criteria for the turbulent-laminar transition has been proposed for Bingham plastic materials (Liu and Mei 1990), and found to be applicable to mud flows. R is composed of viscous (R_μ) and yield-stress (R_τ) components depending on underflow conditions, and

$$R = \frac{1}{\left(1/R_\mu + 1/R_\tau\right)} \text{ where } R_\mu = \frac{4\rho Q}{\mu B} \text{ and } R_\tau = \frac{8\rho Q^2}{\tau_y B^2 h^2} \tag{10}$$

where μ = the apparent viscosity, and τ_y = the yield stress. Experimental evidence indicates that the turbulent-laminar transition occurs at R's of about 2,000 (Liu and Mei 1990; Van Kessel and Kranenburg 1996).

Power law relationships with C were used to specify μ and τ_y. Van Kessel and Kranenburg (1996) and Teeter (1994 and 2000) present some data for laboratory clays such as kaolinite and natural muds. However, data for the range of C measured in this study are scarce. Some data for low-concentration fluid muds from Gulfport Harbor, MS, are presented in Figure 15. Those data were developed from shear-stress sweeps, starting below the yield stress, with a Carri-med controlled-stress rheometer and specially collected samples (Teeter 1993). A concentric cylinder

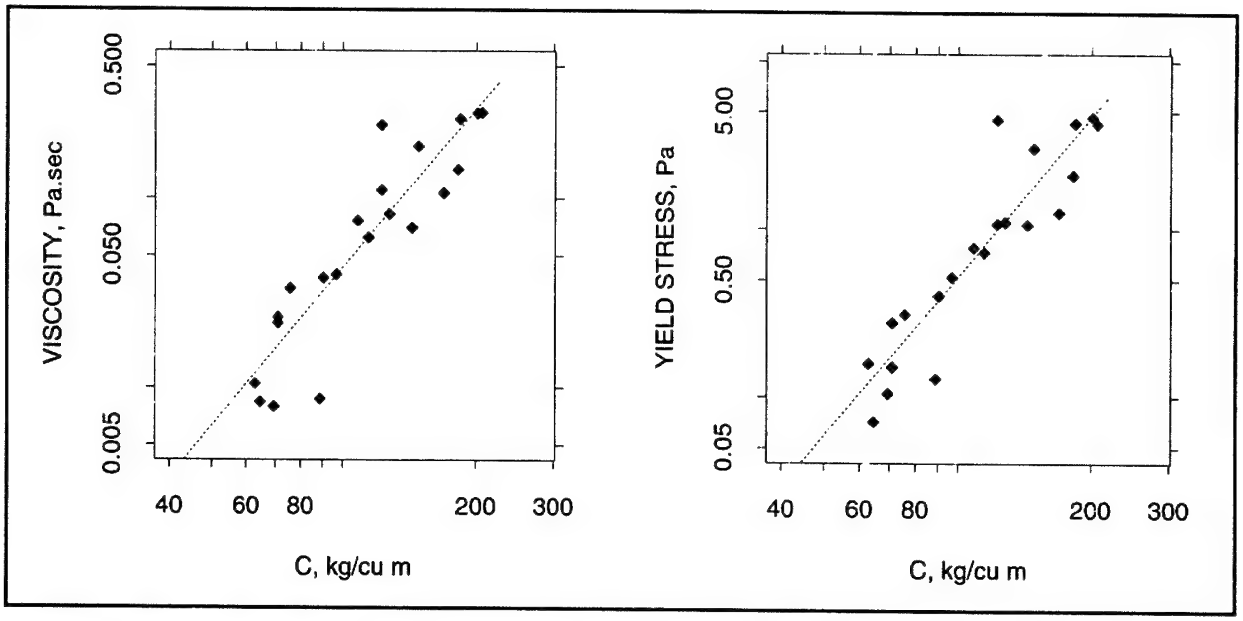

Figure 15. Viscosity at 50 sec^{-1} shear rate and yield stress for fluid mud from Gulfport Harbor, MS

geometry was used, and data fit to a Herschel-Bulkley shear stress model (Coussot 1994) and a Sisko viscosity model (Barnes, Hutton, and Walters 1989).

The yield stresses and viscosities at 50-sec^{-1} shear rate, plotted in Figure 15, are higher for the overlapping range of C than values found for commonly used laboratory clays and other natural muds. Measurements of yield stress were obtained for three channel sediment samples from the GIWW about 6 km north of Port Isabel. The three samples were from the top 7.5 cm of sediment cores and all had densities of about 400 kg/m^3. Yield stresses for these samples, and for other natural muds including Gulfport, are shown in Figure 16. These data indicate that yield stress properties of Laguna Madre mud are not as great as for some other natural muds.

For turbulent conditions, $C_f = gn^2/h^{1/3}$ where n is Manning's friction factor. For laminar conditions, the drag coefficient was estimated as the maximum of the turbulent case or the expression presented by Van Kessel and Kranenburg (1996) for laminar flows:

$$C_f = \frac{12}{R_\mu} + \frac{\tau_y}{\rho U^2} \tag{11}$$

Entrainment. In addition to deposition, entrainment of overlying water can reduce C. A theoretical and laboratory investigation of entrainment was presented by Kranenburg and Winterwerp (1997) and the resulting relationship between entrainment coefficient E_w and Ri tuned for fluid mud by Van Kessel and Kranenburg (1996) is

$$E_w = \frac{5.5 \times 10^{-3}}{3.6\,Ri - 1 + \sqrt{(3.6\,Ri - 1)^2 + 0.15}}, \quad R > 2{,}000 \tag{12}$$

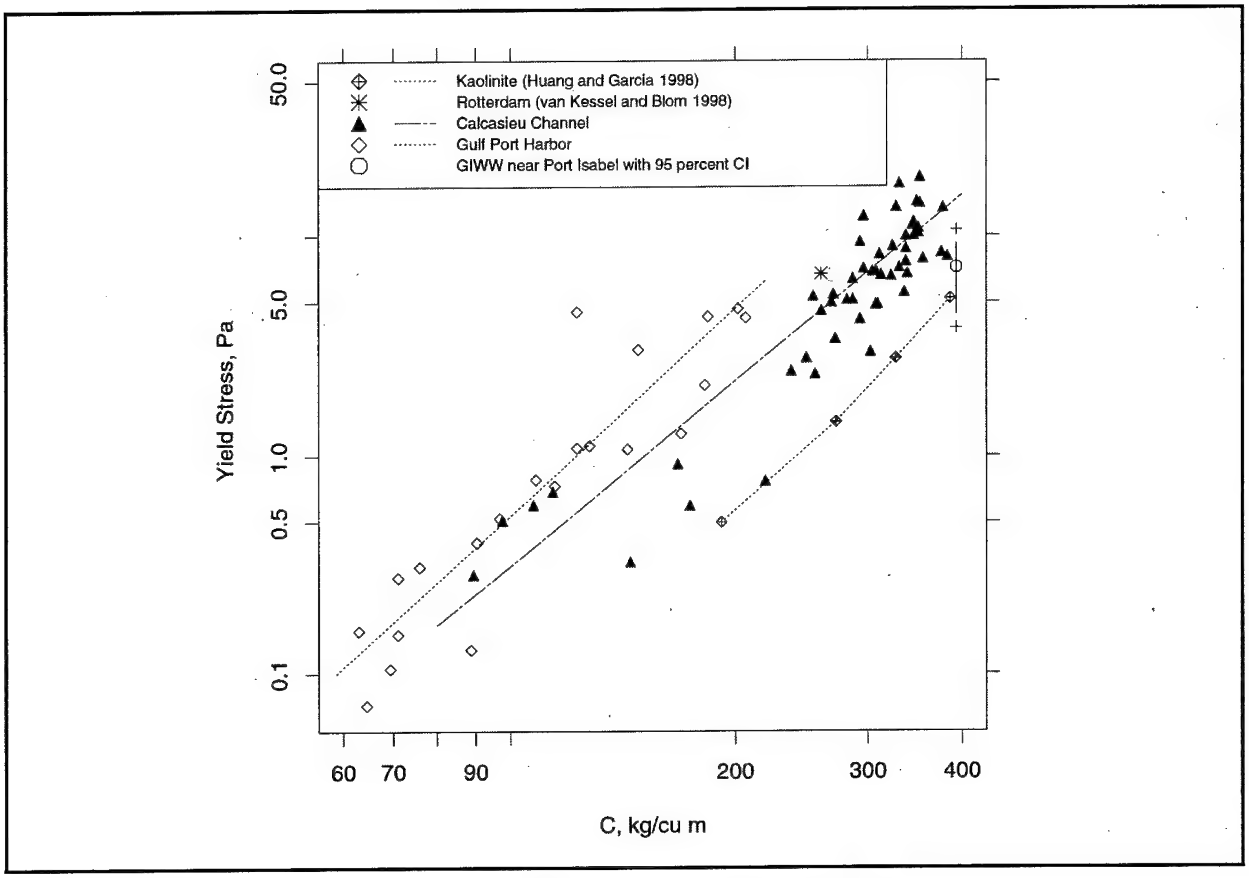

Figure 16. Yield stress for Laguna Madre GIWW sediments and other muds

where Ri is defined in Equation 9 and the condition implies that turbulent flow is required for entrainment to proceed.

Lateral spreading. A buoyant-surface spreading rate developed by Shirazi and Davis (1974) was adopted to the case of negatively-buoyant spreading along the bottom, yielding the expression:

$$\frac{dB}{dx} = 1.4\left(\frac{B}{c_1 h\, Ri} - 1\right)^{-1/2} \tag{13}$$

where c_1 = a coefficient inversely related to the concentration difference. An upper limit of 2.0 was set on dB/dx so that lateral spreading rate could not be larger than the downslope advance rate.

Initial conditions. A flow transition formed the initial condition for the underflow observed on 16 February. A horizontal discharge pipe had a diameter equal to an appreciable fraction of the receiving water depth. A turbulent surface flow was created, which, after some initial entrainment and spreading, plunged to form an underflow in slightly deeper water as shown schematically in Figure 17 and previously in the Figure 8 photograph. The critical Richardson number Ri for a plunging underflow described earlier is slightly greater than 1 (Fang and Stefan 2000).

In addition to the pipeline discharge and discharge concentration (Q_i and C_i), the model requires specification of the initial dilution Sa, initial breadth B_o, and initial Ri which were estimated from field information. The initial height h_o of the underflow was then estimated by

$$h_o = \left(\frac{Q_o}{B_o}\right)^{2/3} \left(\frac{\rho_o Ri_o}{g\Delta\rho_o}\right)^{1/3} \tag{14}$$

where the subscript o refers to values at the underflow transition, $Q_o = SaQ_i$, and $C_o = C_i / Sa$.

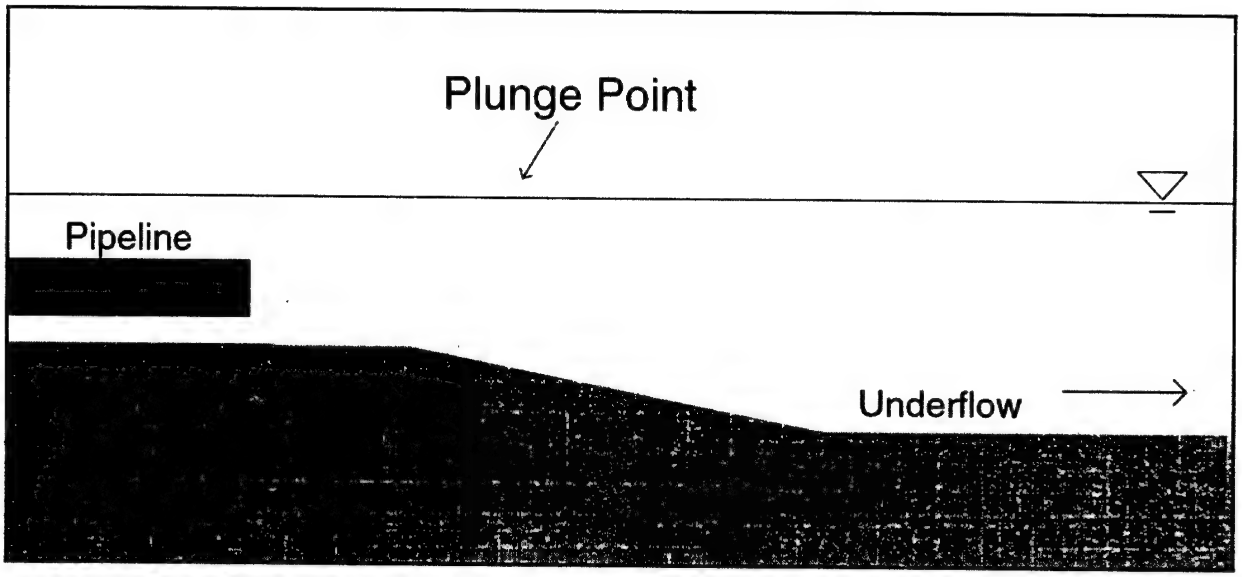

Figure 17. Schematic of shallow horizontal pipeline discharge, turbulent surface flow, and transition to underflow at plunge point

Model Results. Governing and auxiliary equations were used to integrate underflow variables, starting with the initial conditions described in the last section; a fourth-order numerical scheme was used to calculate Q, CQ , B, and h at 1-m intervals along the downslope trajectory of the underflow. Depths from the 1-m contour toward the east-southeast were estimated from sample station and chart depths and interpolated out to a distance of 475 m. Coefficients c_1 and Manning's n were taken as 0.033 and 0.02, and model results were insensitive to the exact values used. Example computed profiles of underflow and deposit heights are shown in Figure 18 for 1 and 6 hr after the discharge began. These results are for B_o = 45 m, Sa = 5.5, initial Ri = 1.5, Q_i = 0.5 m^3/sec, C_i = 100 dry-kg/m^3, τ_{cd} = 0.05 Pa, and the settling properties described previously. The rheological properties were set between those of kaolinite and Gulfport Harbor fluid muds. The downslope extent increased between hours 1 and 6 as the deposit developed and reduced slope between 50- and 150-m x distances. Between hours 1 and 6, breadth-weighted average underflow thickness over the footprint decreased from 0.78 to 0.61 m, the deposit increased from 0.05 to 0.28 m, and the footprint area increased from 19,800 to 24,300 m^2.

The underflow extent in plan view is shown in Figure 19 for hour 6. The most rapid spreading occurred as Ri increased. Spreading abruptly stops where the deposit greatly increases bed slope. The variation of time, velocity, and sediment discharge along x are shown in Figure 20. The

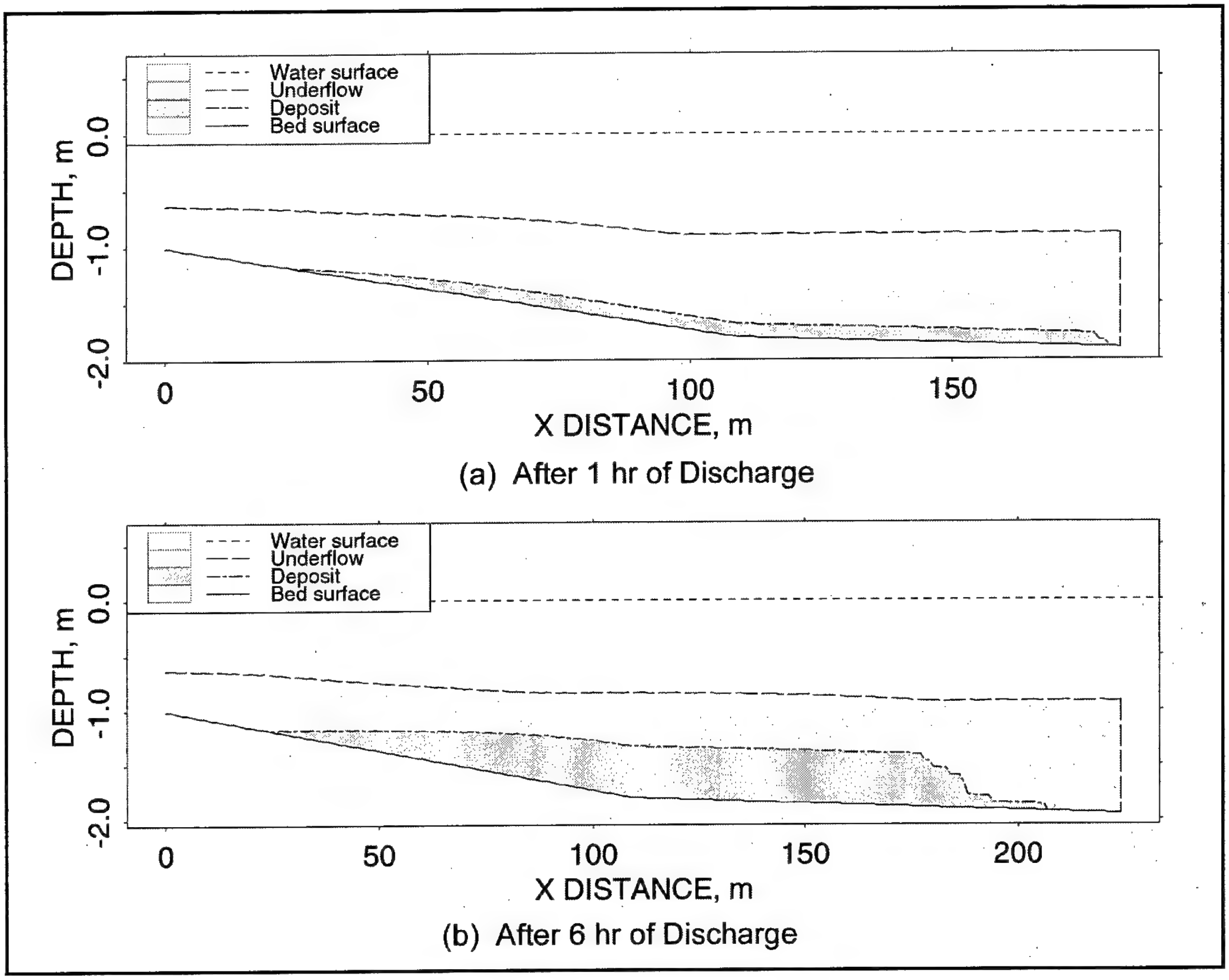

Figure 18. Computed underflow and deposit profiles at two times

underflow velocity decreased rapidly near the origin, then more slowly over the remainder of the x extent. Deposition starts when $U < 0.10$ m/sec. Underflow concentrations were 18 dry-kg/m^3 at the origin and decreased slightly to about 17 dry-kg/m^3 at the maximum downslope extent of the underflow.

ENTRAINMENT INTO WATER COLUMN: Entrainment of material from the underflow into the water column, the reverse of that entrainment previously described, was implied by observed plumes of suspended sediments associated with the location of the underflow footprint. In a deeper estuarine field situation, no such plume was observed by Thevenot, Prickett, and Kraus (1992). Though currents were weak at the Laguna Madre site, winds were relatively strong. The entrainment process depends on the local momentum balance, turbulence at the underflow interface, and the magnitude of density differences. Data collected on 16 February at Laguna Madre were used to make an evaluation of the entrainment process in this section.

Details of the underflow interface with the water column are important to this entrainment process. Either the density step between the water column and the underflow, or, if no such step exists, the gradient at the top of the underflow is used to scale a Richardson number (Turner 1986). As

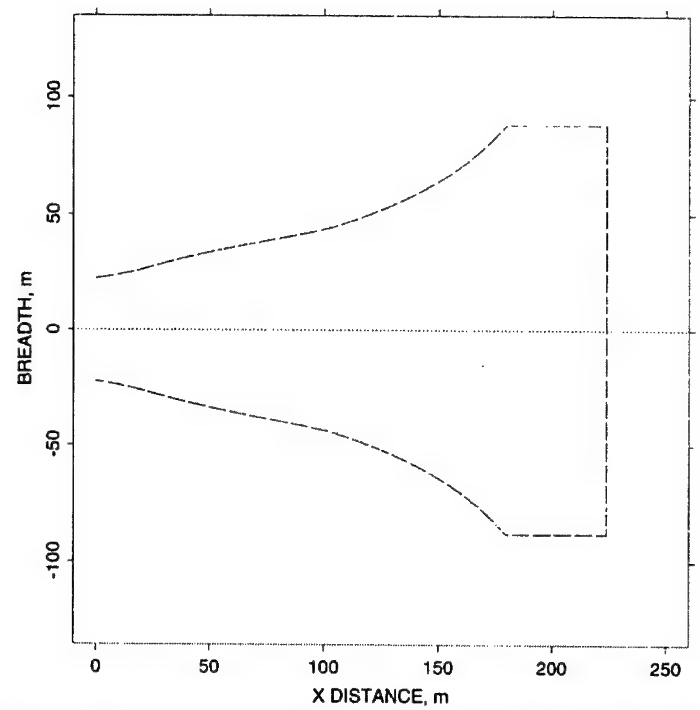

Figure 19. Plan view of computed underflow footprint showing spreading with distance along the x-axis

previously discussed, the underflow was observed to be highly stratified but with a sharp density jump between its upper surface and the overlying water column. Therefore, the magnitude of the jump, along with the depth of the water column above the underflow (H_o), was used to scale a Richardson number. The magnitude of that jump was much smaller than the overall mean density difference between the two layers.

The major momentum input was from the wind. Wind data from a station at Rincon maintained by Texas A&M University, Conrad Blucher Institute, indicated that mean wind speeds at 10-m height (U_a) were 12.0 m/sec for 1000 to 1200 CST on 10 February, and were 7.6 m/sec for 0900 to 1300 CST on 16 February (standard deviations for both time periods were about 1 m/sec). An approximate location for Rincon is given in Figure 1.

Hydrodynamic forcing was assumed to equal the wind stress, some of which goes into waves and some of which goes into currents. Wind-waves in Laguna Madre tend to be at a fully-developed, depth-limited state such that dissipation was nearly equal to the momentum input. Aalderink et al. (1985) compared two models which used wind stress directly with two models which used near-bed wave orbital shear stress, and found that the models which used wind stress directly were better able to match observed TSM. The in-water friction velocity was estimated from

$$u_* = \left(\rho_a C_d / \rho_o\right)^{1/2} U_a \tag{15}$$

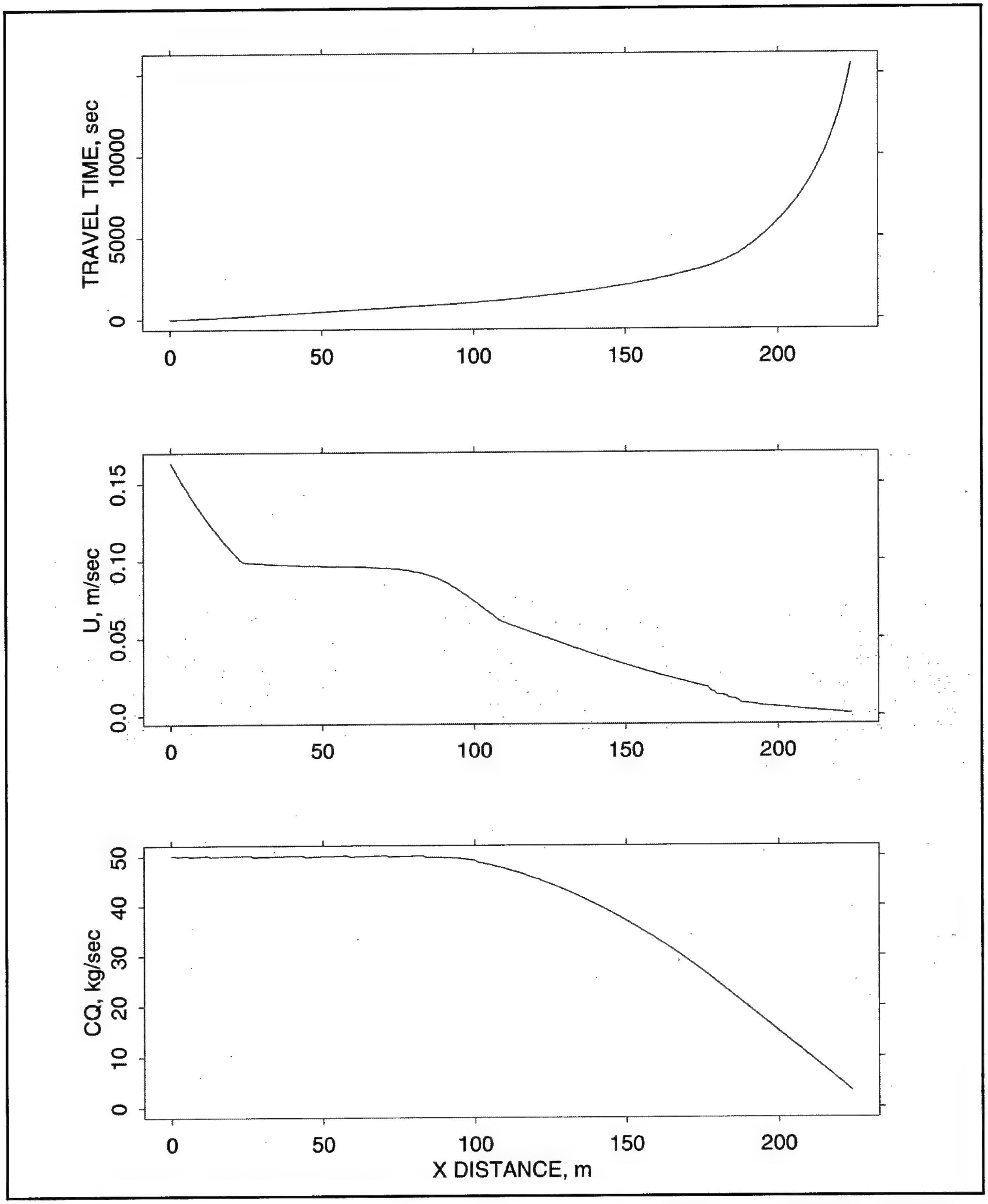

Figure 20. Computed variations of time to reach x distance, underflow velocity, and sediment discharge along the x-axis

where ρ_a and ρ_o are the atmospheric and water column densities and C_d is the shallow-water atmospheric drag coefficient taken as a function of depth and wind speed (Teeter et al. 2001). The average value for u_* on 16 February was about 0.0095 m/sec.

At high interfacial Richardson numbers (Ri_*), dimensionless entrainment (E) is the result of perturbations in the interface between the turbulent water column and the underflow. (Also assuming that the molecular Peclet number = $u_1 l_1/\nu$ is greater than 200 where u_1 and l_1 are the turbulent velocity and length scales, and ν is molecular diffusivity.) Under conditions of turbulence without mean-flow, the laboratory experiments of Long (1975), and E and Hopfinger (1986) confirmed the -3/2 power law described by Linden (1973) that

$$E = \frac{u_e}{u_*} = K\, Ri_*^{-3/2} \tag{16}$$

where u_e is the entrainment velocity or the downward velocity of the interface, K is a constant, and the interfacial Richardson number is defined slightly differently from Ri as

$$Ri_* = \frac{g\,\Delta\rho\, H_o}{\bar{\rho}\, u_*^2} \tag{17}$$

where the density step across the interface $\Delta\rho = (\rho - \bar{\rho})/\bar{\rho}$, $\bar{\rho}$ is the average density of the layers, and H_o is the depth of the water column above the underflow. The scales for $\Delta\rho$ and length can be chosen differently in different entrainment systems. Here, although the underflow is stratified, the mechanism causing that stratification involves settling and not diffusion across an interface. Thicknesses of density interfaces are typically about 6 percent of the depth of mixed layers, much thinner than the stratified underflow layers observed here. Values of Ri_* are large, and interfacial perturbations are probably intermittent, consisting of vortex rebounding. Thus, $\Delta\rho$ and H_o were scaled by the overall density step and the depth of the water column.

Entrainment and deposition to the underflow by settling are assumed to be simultaneous processes in this case. Teeter (1994) reviewed laboratory entrainment experiments involving suspensions and found them to be consistent with an assumption of simultaneous entrainment and settling. Thus, at a depth-averaged water-column point over an underflow

$$H_o \frac{d C_o}{d t} = F_e - F_s \tag{18}$$

where C_o is the depth-averaged suspension concentration in the water column, t is time, and F_e and F_s are the entrainment and settling flux rates at the interface.

A further simplification can be made by assuming that C_o is constant. This assumption is justified since the water-column depth is small, and the time for settling or turbulent mixing is short compared to the time-scales for underflow spread and/or wind speed changes. Under equilibrium conditions of settling and entrainment, F_e and F_s have the same magnitude. Furthermore, the settling flux for

the water suspension can be estimated by use of laboratory settling tests on Laguna Madre channel sediments described by Teeter et al. (in preparation) and shown in Figure 3. These results were obtained by mixing suspensions with site water and allowing them to settle in a 10-cm diam by 1.9-m-tall column under quiescent conditions. Nine initial concentrations were tested, and settling velocity (W_s) was found to increase linearly with initial concentration. A function describing concentration-dependent settling rate for Laguna Madre channel sediments is

$$W_s = \alpha_1 C_o^n, \quad 0.1 < C_o < 1\ \mathrm{kg/m^3} \tag{19}$$

where W_s is in m/sec, $a_1 = 0.806 \times 10^{-3}$ m/sec, and the exponent $n = 1$.

Settling flux depends on depositional probability, as did the depositional flux S described in the last section. Here, turbulence at the interface is assumed to be low and intermittent, and the depositional probability is assumed to be unity. The depositional flux depends on the near bed concentration C_b, but in this case it is assumed that $C_b/C_o \approx 1$. Therefore, $F_e = u_e C$ and $F_s = W_s\, C_o$; a simple model for the water column suspension concentration is

$$C_o = \left(\frac{K}{a_1} C u_* Ri_*^{-3/2}\right)^{1/(n+1)} \tag{20}$$

Equation 20 was recast to solve for the entrainment coefficient K with field data. The Laguna Madre measurements and Equation 7 indicated that $C_b/C_o = 1.07$, and column C_o values were adjusted accordingly. In-water friction-velocities were calculated using Equation 19 and a constant wind speed of 7.6 m/sec. Underflow concentration at the interface was assumed to be 3 dry-kg/m^3. Results for K and other select parameters are presented in Table 2.

The flux Richardson number (Ri_f) was calculated as $(u_e/u_*)Ri_*$ (Turner 1986) and represents the ratio of turbulent kinetic energy dissipation by buoyancy flux and turbulent production. Flux Richardson numbers greater than 0.1 are associated with damping of turbulence, and the magnitudes of Ri_f obtained here indicate appreciable suppression of turbulence at the interface.

The K (and TSM) values were log-normally distributed. The median K value was 2.8 in fair agreement with the laboratory result of 3.8 reported by E and Hopfinger (1986). Based on this estimate for K, an estimate of C_o was made for 10 February with Equation 20. Assuming underflow conditions were the same as before, where $\Delta\rho/\bar{\rho} = 0.00081$, , and that $H_o = 2$ m and $u_* = 0.0174$ m/sec, then the Ri_* for that day was about 52. Equation 20 predicts $C_o = 690$ mg/L or somewhat higher than the high values observed in the field (Figure 5).

DISCUSSION AND CONCLUSIONS: Some of the important results from the field measurements were as follows: the underflow thickness was relatively uniform and decreased rapidly near the limit of downslope extent. The underflow had a distinct upper surface or interface with the ambient water column, but this concentration was only about 3 dry-kg/m^3. Underflow layers were sediment and density stratified. Turbulence in the underflow was not sufficient to mix sediment vertically. Thick deposits formed under the underflow. The implication of these observations was that the underflow was slow moving. An apparent absence of appreciable entrainment also indicated

Table 2
Entrainment Conditions at Underflow Profile Stations

Time, CST	TSM, mg/L	H_o, m	Ri_*	$F_s \times 10^5$ kg/m^2/sec	K	Ri_f
1057	168	0.86	86	2.6	0.7	0.1
1110	240	0.26	133	5.3	2.8	0.2
1122	308	0.41	69	8.8	1.8	0.2
1136	228	0.37	128	4.8	2.4	0.2
1216	480	0.29	134	21.3	11.4	1
1233	708	0.2	124	46.3	22.1	2
1308	260	0.25	151	6.2	4	0.3

slow underflow movement and high Richardson numbers. The concentrations near this upper surface and layer average values were relatively uniform along the length of the underflow. This observation indicated the underflow collapsed vertically while depositing and led to the model feature that tended to maintain underflow concentrations while deposition occurred.

The results from the model were in general agreement with features observed in the field. The model predicted the underflow to be slow moving, starting turbulent and becoming laminar after 85 to 150 m distance downslope. Calculated underflow concentrations were almost constant. Deposition started near the source, became appreciable after 100 m, and decreased rapidly at the downslope extent of the underflow. Underflow thicknesses in the model were similar to those observed in the field. The extent of the underflow could not be accurately measured in the field but appeared to be in rough agreement with the model predictions. Lateral spreading, which was controlled by bed topography, was captured only in a very approximate way in the model. The model did not include path switching that apparently occurred in the field nor the complexity of bottom topography that influences underflow spreading.

Laboratory-determined settling velocities were used in the description of underflow spreading and in the analysis of water column entrainment of underflow material. Laboratory measured values are probably not the same as field values, but obtaining measurements in the field is problematic. Teeter (2001) showed that for low-concentration Laguna Madre suspended sediments, quiescent column tests yielded settling rates representative of disrupted flocs. Very mild turbulence produced much larger values, but shear rates greater than 2 sec^{-1} produced settling rates that were not much different from quiescent values. The uncertainty in W_s affects the results of both the underflow and water column analyses, if performed in a predictive mode.

Our understanding of fluid-mud flow properties is incomplete and measurements are difficult. The existence of a yield stress may lead to an unsheared plug flow zone (Coussot 1994) in the underflow and could make R values based on layer average properties unrepresentative of interface conditions where entrainment occurs. In the present case, the underflow layer was highly stratified, and the velocity profile was difficult to evaluate. The flow-regime evaluation imposed on Equation 12 only captures the effect of fluid-mud flow properties on entrainment, if such properties are known or can be estimated.

Rheological data on muds are relatively scarce. While varying rheological parameters over an order of magnitude from those used in the example calculation did not greatly affect results, increases in viscous and yield stress properties eventually caused the model underflow to freeze and become numerically unstable. The range from laboratory clays to cohesive natural muds such as those in Figures 15 and 16 affect computed underflow *R*, friction, flow, and ultimate extent of spreading. The predictive capability of the model is therefore dependent on rather extensive site-specific field information. Important factors include sediment composition, settling and rheological characteristics, bed topography, ambient currents, winds, and waves.

Elevated water-column suspended sediment concentrations were caused by underflow entrainment into the water column by wind-wave forcing. Entrainment model coefficients were consistent with previously reported values for high Ri_* situations when used with wind-stress forcing.

The pipeline discharge underflow represents the greatest potential for local turbidity generation, if it is entrained into the overlying flow, since it contains the vast majority of sediment particles discharged. Field observations indicate that at times of high bed shear-stress, entrainment of underflow material can generate a turbid plume extending some distance from the discharge, but not necessarily downstream from the discharge. Thus, the area of concern with respect to water column impacts of a pipeline discharge is not confined to the vicinity of discharge, but also includes the area over the underflow that might extend hundreds of meters.

ACKNOWLEDGMENTS: The field work was arranged with assistance of Mr. Joe Hramates of the U. S. Army Engineer District, Galveston, and supported under the Dredging Operations and Environmental Research Program (DOER) of the U.S. Army Corps of Engineers. Mr. David Thomas of PBS&J, Inc., a Galveston District contractor from Austin, TX, expertly operated the boat and assisted with sampling during sometimes difficult field conditions.

POINTS OF CONTACT: For additional information, contact Dr. Allen Teeter (601-634-2820, *teeter@hl.wes.army.mil*), or the Program Manager of the Dredging Operations Environmental Research Program, Dr. Robert Engler (601-634-3624, *Robert.M.Engler@erdc.usace.army.mil*).
This technical note should be cited as follows:

> Teeter, A. M. (2002). "Sediment dispersion near dredge pipeline discharge in Laguna Madre, Texas," *DOER Technical Notes Collection* (ERDC TN-DOER-N16), U.S. Army Research and Development Center, Vicksburg, MS. *www.wes.army.mil/el/dots/doer*

REFERENCES

Aalderink, R. H., Lijklema, L., Breukelman, J., van Raaphost, W., and Brinkman, A.G. (1985). "Quantification of wind induced resuspension in a shallow lake," *Wat. Sci. Technol.* 17, 903-914.

Barnes, H. A., Hutton, J. F., and Walters, K. (1989). *An introduction to rheology*. Elsevier, Amsterdam.

Burd, A. B., and Dunton, K. H. (2000). "Field verification of a light-driven model of biomass changes in the seagrass *Halodule Wrightii*," University of Texas, Austin, TX.

Brown, C. A., and Kraus, N. C. (1997). "Environmental monitoring of dredging and processes in Lower Laduna Madre, Texas," Technical Report TAMU-CC-CBI-96-01, Texas A&M University, Corpus Christi, TX.

Coussot, P. (1994). "Steady, laminar, flow of concentrated mud suspensions in open channel," *J. Hydraulic Res.* 32(4), 535-559.

Dunton, K. H. (1994). "Seasonal growth and biomass of the tropical seagrass *Halodule wrightii* in relation to continuous measurements of underwater irradiance," *Marine Biology* 120, 479-489.

E, X., and Hopfinger, E. J. (1986). "On mixing across an interface in stably stratified fluid," *J. Fluid Mech.* 166, 227-244.

Ellison, T. H., and Turner, J. S. (1959). "Turbulent entrainment in stratified flows," *J. Fluid Mech.* 6, 423-448.

Fang, X., and Stefan, H. G. (2000). "Dependence of dilution of a plunging discharge over a sloping bottom on inflow conditions and bottom friction," *J. Hydraulic Res.* 38(1): 15-25.

Findikakis, A. N., and Law, A. W. K. (1998). "Marine tailings disposal simulation," *J. Hydraulic Engrg.* 24(4), 370-383.

Kranenburg, C., and Winterwerp, J. (1997). "Erosion of fluid mud layers, Part I: Entrainment model," *J. Hydraulic Engrg.* 123(6), 504-511.

Huang, X., and Garcia, M. H. (1998). "A Herschel-Bulkley model for mud flow down slope," *J. Fluid Mech.* 374, 305-333.

Liu, K. F., and Mei, C. C. (1990). "Approximate equations for the slow spreading of a thin sheet of Bingham plastic fluid," *Physics of Fluids* A2(1), 30-36.

Long, R. F. (1975). "The influence of shear on mixing across density interfaces," *J. Fluid Mech.* 70(2), 305-320.

Linden, P. F. (1973). "The interaction of a vortex ring with a sharp density interface: A model for turbulent entrainment," *J. Fluid Mech.* 60, 467-480.

Militello, A., Kraus, N. C., and Kite, R. D., Jr. (1997). "Environmental monitoring of dredging and processes in the Upper Laguna Madre, TX," Technical Report, TAMU-CC-CBI-97-03, Texas A&M University, Corpus Christi, TX.

Morton, R. A., Nava, R. C., and Arhelgar, M. (2001). "Factors controlling navigation channel shoalling in Laguna Madre, TX," *J. Waterw., Port, Coast., and Ocean Engrg.* 127(2), 72-81.

Onuf, C. P. (1994). "Seagrasses, dredging, and light in Laguna Madre, TX, USA," *Estu., Coast., Shelf Sci.* 39, 75-91.

Panageotou, W., and Halka, J. (1990). "Monitoring of sediment dredged from the approach channel to the Chesapeake and Delaware Canal November, 1988 - September, 1989," Open File Report 10, Maryland Geological Survey, Baltimore, MD.

Panageotou, W., and Halka, J. (1994). "Studies of dredged sediments placed in open-water sites in the northern Chesapeake Bay October, 1991 - March, 1992", File Report 94-1, Maryland Geological Survey, Baltimore, MD.

Parker, G., Fukushima, Y., and Pantin, H. M. (1986). "Self-accelerating turbidity currents," *J. Fluid Mech.* 171, 145-181.

Shirazi, M. A., and Davis, L. R. (1974). "Workbook for thermal plume prediction. Volume 2: Surface discharge," Report EPA-R2-72-005b, U.S. Environmental Protection Agency, Corvallis Environ. Res. Laboratory, Corvallis, OR.

Teeter, A. M. (1986). "Veretical transport in fine-grained suspension and newly-deposited sediment," *Estuarine cohesive sediment dynamics*. A.J. Mehta, ed., Springer-Verlag, New York, 170-191.

Teeter, A. M. (1993). "Navigability criterion for Gulfport Harbor, Mississippi," CEWES-HE Memorandum to U.S. Army Engineer District, Mobile, U.S. Army Engineer Waterways Experiment Station, Vicksburg, MS.

Teeter, A. M. (1994). "Erosion by entrainment of fluidized cohesive sediments," Technical Note DRP-1-15, U.S. Army Engineer Waterways Experiment Station, Vicksburg, MS.

Teeter, A. M. (2000). "Underflow spreading from an open-pipeline disposal," *DOER Technical Notes Collection* (ERDC TN-DOER-N7), U.S. Army Engineer Research and Development Center, Vicksburg, MS.

Teeter, A. M. (2001). "Clay-silt sediment modeling using multiple grain classes. Part I: Settling and deposition," *Coastal and etuarine fine sediment processes*. W.H. McAnally and A.J. Mehta, ed., Elsevier, Amsterdam, 157-171.

Teeter, A. M., Johnson, B. H., Berger, C., Stelling, G., Scheffner, N. W., Garcia, M. H., and Parchure, T. M. (2001). "Hydrodynamic and sediment transport modeling with emphasis on shallow-water, vegetated areas (lakes, reservoirs, estuaries and lagoons)," *Hydrobiologia* 444, 1-23.

Teeter, A. M., Brown, G., Alexander, M., Callegan, C., Sarruff, M. S., and McVan, D. (in preparation). "Wind-wave resuspension and circulation of sediment and dredged material in Laguna Madre, TX," Technical Report, U.S. Army Engineer Research and Development Center, Vicksburg, MS.

Thevenot, M. M., Prickett, T. L., and Kraus, N. C. (1992). "Tylers Beach, Virginia, dredged material plume monitoring project: 27 Septmeber to 4 October 1991," Technical Report DRP-92-7, U.S. Army Engineer Waterways Experiment Station, Vicksburg, MS.

Turner, J. S. (1986). "Turbulent entrainment: The development of the entrainment assumption, and its application to geophysical flows," *J. Fluid Mech.* 173, 431-471.

Van Kessel, T., and Blom, C. (1998). "Rheology of coheisve sediments: Comparison between natural and an artificial mud," *J. Hydraulic Res.* 36(4), 591-612.

Van Kessel, T., and Kranenburg, C. (1996). "Gravity current of fluid mud on sloping bed," *J. Hydraulic Engrg.* 122(12), 710-717.

Wolanski, E., Gibbs, J. J., Mazda, Y., Mehta, A., and King, B. (1992). "The role of turbulence in the settling of mud flocs," *J. Coastal Res.* 8(1), 35-46.